Frequency Diverse Coprime Arrays with Coprime Frequency Offsets for Multi-Target Localization

Si Qin, *Student Member, IEEE*, Yimin D. Zhang, *Senior Member, IEEE*, Moeness G. Amin, *Fellow, IEEE*, and Fulvio Gini, *Fellow, IEEE*

***Abstract*—Different from conventional phased-array radars, the frequency diverse array (FDA) radar offers a range-dependent beampattern capability that is attractive in various applications. The spatial and range resolutions of an FDA radar are fundamentally limited by the array geometry and the frequency offset. In this paper, we overcome this limitation by introducing a novel sparsity-based multi-target localization approach incorporating both coprime arrays and coprime frequency offsets. The covariance matrix of the received signals corresponding to all sensors and employed frequencies is formulated to generate a space-frequency virtual difference coarrays. By using $\mathcal{O}(M+N)$ antennas and $\mathcal{O}(M+N)$ frequencies, the proposed coprime arrays with coprime frequency offsets enables the localization of up to $\mathcal{O}(M^2N^2)$ targets with a resolution of $\mathcal{O}(1/(MN))$ in angle and range domains, where M and N are coprime integers. The joint direction-of-arrival (DOA) and range estimation is cast as a two-dimensional sparse reconstruction problem and is solved within the Bayesian compressive sensing framework. We also develop a fast algorithm with a lower computational complexity based on the multitask Bayesian compressive sensing approach. Simulations results demonstrate the superiority of the proposed approach in terms of DOA-range resolution, localization accuracy, and the number of resolvable targets.**

***Index Terms*—Target localization, frequency diverse array radar, coprime array, coprime frequency offset, Bayesian compressvie sensing**

I. Introduction

Target localization finds a variety of applications in radar, sonar, communications, and navigation [2]–[5]. The phased array radars are known for their capability to electronically steer a beam for target detection and tracking in the angular domain [6]–[9]. To localize targets in both angle and range, beam-steering should be achieved across a signal bandwidth. This generally leads to a complicated waveform design and signal processing algorithms. Recently, the frequency diverse array (FDA) framework was introduced as an attractive multiple-input multiple-output (MIMO) structure that performs beam steering over a signal bandwidth and achieves joint estimation of targets direction-of-arrival (DOA) and range information [10]–[20]. As compared with conventional arrays that assume a fixed carrier frequency, FDA radars use a small frequency increment across array elements and thus achieve beam steering as a function of the angle and range in the far field. In FDA radars, the spatial and range resolutions are fundamentally limited by the array aperture and maximum frequency increment. In addition, the number of degrees-of-freedom (DOFs) offered by the array sensors and frequency increments determines the maximum number of detectable targets.

The traditional FDA exploits a uniform linear array with a uniform frequency offset. The range and DOA estimation problem using such FDA radar has been discussed in [21]–[23]. In [21], [22], the target ranges and DOAs are jointly estimated by the minimum variance distortionless response (MVDR) and the MUSIC methods, respectively. Unlike [21], [22], an FDA utilizing coherent double pulse respectively with zero and non-zero frequency increments is considered in [23], where the ranges and DOAs are estimated in two steps. In the zero frequency increment case, the DOAs are first estimated using a non-adaptive beamformer. The estimated DOA information is then used as the prior knowledge by adaptive beamforming to obtain the range information in the other pulse. It is important to note that the above methods [21]–[23] use the traditional FDA radar and are discussed in the physical sensor framework rather than the virtual difference coarray. That is, for an array with N_t sensors, there are only $\mathcal{O}(N_t)$ DOFs with a resolution $\mathcal{O}(1/N_t)$ in both the range and angle domains. While the angular and range resolutions can be improved by exploiting a large interelement spacing and a large frequency increment, such structure generally requires a large number of array sensors, or otherwise yields undesirable aliasing problems, i.e., causes ambiguous estimations in angular and range dimensions.

Compared with uniform linear arrays (ULAs), sparse arrays use the same number of sensors to achieve a larger array aperture. A properly designed non-uniform array can achieve a desired trade-off between meanbeam width and sidelobe levels and, thereby, provide enhanced performance in terms of DOA accuracy and resolution. These attributes are achieved without changes in size, weight, power consumption, or cost. More importantly, sparse arrays offer a higher number of DOFs through the exploitation of the coarray concept [24] and, as such, significantly increases the number of detectable targets. Likewise, non-uniform frequency offsets can be used to achieve improved target identifiability and resolution in the

The work of S. Qin, Y. D. Zhang, and M. G. Amin was supported in part by the Office of Naval Research under Grant No. N00014-13-1-0061. Part of the results was presented at the IEEE Radar Conference, Philadelphia, PA, May 2016 [1].

S. Qin and M. G. Amin are with the Center for Advanced Communications, Villanova University, Villanova, PA 19085, USA.

Y. D. Zhang is with the Department of Electrical and Computer Engineering, Temple University, Philadelphia, PA 19122, USA.

F. Gini is with Department of Information Engineering of the University of Pisa, 56122 Pisa, Italy.

The corresponding author's email address is ydzhang@temple.edu.

range dimension [25]. Among different techniques that are available for sparse signal structures and array aperture synthesis, the recent proposed nested [26] and coprime configurations [27] offer systematical design capability and DOF analysis involving sensors, samples, or frequencies [28]–[41].

In [42], a nested array is employed to generate a coarray where the MUSIC algorithm together with spatial smoothing is applied. As a result, the number of the DOFs in the angular domain is increased to $\mathcal{O}(N_t^2)$. In [43], a sparsity-based method using the nested array is proposed. It achieves improved resolution and estimation accuracy when compared with the conventional covariance based methods. However, the number of the DOFs in the range domain is still $\mathcal{O}(N_t)$ since a uniform frequency offset is used. In addition, due to the large dimension of the joint range and angle dictionary, this method results in a prohibitive computational complexity that limits its practical applicability, particularly when the number of antennas is large.

In this paper, we propose a novel configuration for the FDA radar, which incorporates both coprime array structure and coprime frequency offsets. In the proposed approach, the offsets of carrier frequencies assume a coprime relationship to further increase the number of DOFs beyond that achieved by only implementing the sparse arrays with uniform frequency increments. As a result, by using $\mathcal{O}(N_t)$ antennas and $\mathcal{O}(N_t)$ frequencies, the proposed approach achieves $\mathcal{O}(N_t^2)$ DOFs with a resolution of $\mathcal{O}(1/N_t^2)$ in both angular and range domains.

In this paper, we consider point-like targets and we exploit their sparsity in both range and angular domains. We propose both joint and sequential estimation methods based on the space-frequency coarray structure. For the joint estimation, the covariance matrix of the received signals corresponding to all sensors and employed frequencies is formulated to generate a virtual difference coarray structure in the joint space-frequency domain. Then, a joint-variable sparse reconstruction problem in the range and angular domain is presented as a single measurement vector (SMV) model. We further develop a novel sequential two-step algorithm in the context of group sparsity for reduced complexity. The cross-covariance matrices between the signals received at all sensors corresponding to different frequency pairs form space-only coarrays. Observations in these coarrays exhibit a group sparsity across all frequency pairs, since their sparse angular domain vectors share the same non-zero entry positions associated with the same target DOAs. Therefore, the DOAs can be first solved under a multiple measurement vector (MMV) model. The values of nonzero entries contain the range information, and their estimates across all frequency pairs are utilized to formulate a sparse reconstruction model with respect to the range. In so doing, the joint DOA and range estimation problem is recast as two sequential one-dimensional (1-D) estimation problems with a significantly reduced computational complexity.

The above sparse learning problems can be solved within the compressive sensing (CS) framework [44] and various CS methods can be used for this purpose. As a preferred approach, we exploit the algorithms developed in the sparse Bayesian learning context as they achieve superior performance and are insensitive to the coherence of dictionary entries [45]–[51]. In particular, the complex multitask Bayesian compressive sensing (BCS) method [45], which effectively handles complex-value observations in the underlying problem, is used in this paper.

The main contribution of this work is threefold: (a) We achieve a significantly increased number of DOFs and improve both angular and range resolutions by exploiting both coprime array and coprime frequency offsets under the coarray and frequency difference equivalence. (b) We employ a sparsity-based method to solve the joint DOA and range estimation problem which, when compared to conventional MUSIC-based approach, enables more effective utilization of the available coarray aperture and frequency differences to resolve a higher number of targets and improve the localization accuracy. (c) We further develop a group-sparsity based algorithm which, by casting the joint DOA and range estimation as two sequential 1-D estimation problems, significantly reduces the computational complexity and processing time.

The rest of the paper is organized as follows. In Section II, the signal model of the traditional FDA radar is described. In Section III, we present a new FDA structure using coprime arrays and coprime frequency offsets. By effectively utilizing the available coarray aperture and frequency differences, two sparsity-based multi-target localization methods are proposed in Sections IV and V that resolve a higher number of targets and improve the localization accuracy. More specifically, in Section IV, the DOA and range are jointly estimated by a two-dimensional (2-D) sparse reconstruction algorithm, whereas a low-complexity algorithm through sequential 1-D sparse reconstruction is presented in Section V. Simulation results are provided in Section VI to numerically compare the localization performance of the proposed approach with other methods in terms of the number of resolvable targets, DOA-range resolution, and localization accuracy. Such results reaffirm and demonstrate the effectiveness of the proposed approach. Section VII concludes the paper.

Notations: We use lower-case (upper-case) bold characters to denote vectors (matrices). In particular, $\mathbf{I}_N$ denotes the $N \times N$ identity matrix. $(.)^*$ implies complex conjugation, whereas $(.)^T$ and $(.)^H$ respectively denote the transpose and conjugate transpose of a matrix or vector. $\mathrm{vec}(\cdot)$ denotes the vectorization operator that turns a matrix into a vector by stacking all columns on top of the another, and $\mathrm{diag}(\mathbf{x})$ denotes a diagonal matrix that uses the elements of $\mathbf{x}$ as its diagonal elements. $\mathrm{E}(\cdot)$ is the statistical expectation operator and $\otimes$ denotes the Kronecker product. $P_r(\cdot)$ denotes the probability density function (pdf), and $\mathcal{N}(x|a,b)$ denotes that random variable x follows a Gaussian distribution with mean a and variance b. Similarly, $\mathcal{CN}(a,b)$ denotes joint complex Gaussian distribution with mean a and variance b. $\Gamma(\cdot)$ is the Gamma function operator. $\delta_{q,p}$ is a delta function that returns the value of 1 when $p = q$ and 0 otherwise. $\mathbb{N}$ and $\mathbb{N}^+$ respectively denote the set of non-negative integers and positive integers, whereas $\mathbb{R}^+$ denotes the set of positive real numbers. $|\cdot|$ denotes the determinant operation, whereas $\|\cdot\|_2$ and $\|\cdot\|_F$ represent the Euclidean (l_2) norm and Frobenious norm, respectively. $\mathrm{Tr}(\mathbf{A})$ returns the trace of matrix $\mathbf{A}$.

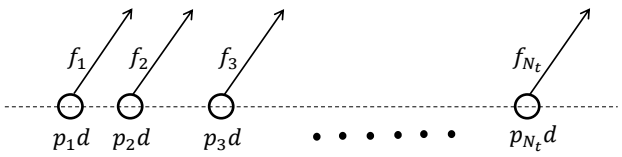

Fig. 1. The FDA configuration.

II. Frequency Diverse Array Radar

Without loss of generality, we limit our discussion to far-field targets in the 2-D space where the DOA is described by the azimuth angle only. Extension to three-dimensional (3-D) space is straightforward.

A. Signal Model

As shown in Fig. 1, an FDA radar utilizes a linear array with N_t antennas. Note that the array spacing can be either uniform or non-uniform. Denote $\mathbf{p} = [p_1 d, ..., p_{N_t} d]^T$ as the positions of the array sensors where $p_k \in \mathbb{N}$, $k = 1, ..., N_t$. The first sensor, located at $p_1 = 0$, is used as the reference. To avoid spatial ambiguity, d is typically taken as half wavelength, i.e., $d = \lambda_0/2 = c/(2f_0)$, where c is the velocity of electromagnetic wave propagation and f_0 is the base carrier frequency. Different from the conventional phased-array radar where all antennas transmit the same signal with carrier frequency f_0, each FDA element radiates a signal with an incremental carrier frequency. That is, a continuous-wave (CW) signal transmitted from the kth element is expressed as

$$s_k(t) = A_k \exp(j2\pi f_k t), \tag{1}$$

where A_k is the amplitude and the radiation frequency $f_k = f_0 + \xi_k \Delta f$ is exploited with a unit frequency increment Δf, and $\xi_k \in \mathbb{N}$ is an integer coefficient of the frequency offset applied at the kth element, $k = 1, ..., N_t$. The maximum increment is assumed to satisfy $\xi_{N_t} \Delta f \ll f_0$ so as to guarantee that the FDA radar works in a narrowband platform. Also, the frequency offsets are not necessary uniform.

An important objective of this paper is to improve the parameter identifiability using the FDA radar. Since the targets in different bins can be simple identified, we consider a scene with Q far-field targets within the same Doppler bin. Without loss of generality, the Doppler frequency is assumed to be 0. The locations of the targets are modeled as (θ_q, R_q), $q = 1, 2, \cdots, Q$. Then, the received signal at the lth sensor is modeled as

$$\begin{aligned}\breve{x}_l(t) =& \sum_{k=1}^{N_t} \sum_{q=1}^{Q} \rho_q(t) \exp(j2\pi f_k t) e^{-j\frac{4\pi}{\lambda_k} R_q} e^{-j\frac{2\pi p_l d}{\lambda_k} \sin(\theta_q)} \\ &+ \breve{n}_l(t), \quad l = 1, \ldots, N_t,\end{aligned} \tag{2}$$

where $\rho_q(t), q = 1, \ldots, Q$, are complex scattering coefficients of the targets, which are assumed to be uncorrelated zero-mean random variables with $\mathrm{E}[\rho_q^* \rho_p] = \sigma_q^2 \delta_{q,p}, 1 \le q, p \le Q$, due to, e.g., the radar cross section (RCS) fluctuations. In addition, $\lambda_k = c/f_k$ denotes the wavelength corresponding to carrier frequency f_k. Furthermore, $\breve{n}_l(t)$ is the additive noise, which is assumed to be spatially and temporally white, and is independent of target signals.

By implementing the pass-band filtering, the received signal is converted to the signals corresponding to the respective frequencies. For a CW waveform with frequency f_k transmitted from the kth sensor, the baseband signal received at the lth sensor can be expressed as

$$\begin{aligned}x_{k,l}(t) =& \sum_{q=1}^{Q} \rho_q(t) e^{-j\frac{4\pi}{\lambda_k} R_q} e^{-j\frac{2\pi p_l d}{\lambda_k} \sin(\theta_q)} + n_{k,l}(t) \\ =& \sum_{q=1}^{Q} \rho_q(t) e^{-j\frac{4\pi f_k}{c} R_q} e^{-j\frac{\pi p_l (f_0 + \xi_k \Delta f)}{f_0} \sin(\theta_q)} + n_{k,l}(t),\end{aligned} \tag{3}$$

where $n_{k,l}(t)$ is the noise at the filter output with a variance σ_n^2. Because $\xi_k \Delta f \ll f_0$, the above expression can be simplified as

$$x_{k,l}(t) = \sum_{q=1}^{Q} \rho_q(t) e^{-j\frac{4\pi f_k}{c} R_q} e^{-j\pi p_l \sin(\theta_q)} + n_{k,l}(t). \tag{4}$$

Stacking $x_{k,l}(t)$ for all $k, l = 1, ..., N_t$ yields an $N_t^2 \times 1$ vector,

$$\begin{aligned}\mathbf{x}(t) &= \sum_{q=1}^{Q} \rho_q(t) \mathbf{a}_{p,f}(\theta_q, R_q) + \mathbf{n}(t) \\ &= \mathbf{A}_{p,f} \mathbf{d}(t) + \mathbf{n}(t),\end{aligned} \tag{5}$$

where $\mathbf{a}_{p,f}(\theta_q, R_q) = \mathbf{a}_p(\theta_q) \otimes \mathbf{a}_f(R_q)$ represents the steering vector associated with the angle-range pair (θ_q, R_q). Herein, $\mathbf{a}_p(\theta_q)$ and $\mathbf{a}_f(R_q)$ are steering vectors corresponding to θ_q and R_q, respectively, expressed as

$$\mathbf{a}_p(\theta_q) = \left[1, e^{-j\pi p_2 \sin(\theta_q)}, \cdots, e^{-j\pi p_{N_t} \sin(\theta_q)}\right]^T, \tag{6}$$

$$\mathbf{a}_f(R_q) = \left[e^{-j\frac{4\pi f_1}{c} R_q}, e^{-j\frac{4\pi f_2}{c} R_q}, \cdots, e^{-j\frac{4\pi f_{N_t}}{c} R_q}\right]^T. \tag{7}$$

In addition, $\mathbf{A}_{p,f} = [\mathbf{a}_{p,f}(\theta_1), \cdots, \mathbf{a}_{p,f}(\theta_Q)]$, $\mathbf{d}(t) = [\rho_1(t), \cdots, \rho_Q(t)]^T$, and $\mathbf{n}_k(t)$ is the noise vector following the joint complex Gaussian distribution $\mathcal{CN}(0, \sigma_n^2 \mathbf{I}_{N_t^2})$.

The $N_t^2 \times N_t^2$ covariance matrix of data vector $\mathbf{x}(t)$ is obtained as

$$\begin{aligned}\mathbf{R}_{\mathbf{x}} &= \mathrm{E}[\mathbf{x}(t)\mathbf{x}^H(t)] = \mathbf{A}_{p,f} \mathbf{R}_{\mathbf{dd}} \mathbf{A}_{p,f}^H + \sigma_n^2 \mathbf{I}_{N_t^2} \\ &= \sum_{q=1}^{Q} \sigma_q^2 \mathbf{a}_{p,f}(\theta_q, R_q) \mathbf{a}_{p,f}^H(\theta_q, R_q) + \sigma_n^2 \mathbf{I}_{N_t^2},\end{aligned} \tag{8}$$

where $\mathbf{R}_{\mathbf{dd}} = \mathrm{E}[\mathbf{d}(t)\mathbf{d}^H(t)] = \mathrm{diag}([\sigma_1^2, \ldots, \sigma_Q^2])$ represents the target scattering power. Note that we assume the target scattering coefficients to be frequency-independent for the emitting signals since the frequency offsets are relatively small. In practice, the covariance matrix is estimated using T available samples, i.e.,

$$\hat{\mathbf{R}}_{\mathbf{x}} = \frac{1}{T} \sum_{t=1}^{T} \mathbf{x}(t)\mathbf{x}^H(t). \tag{9}$$

Existing covariance matrix based techniques can then be applied to estimate the DOA and range of the targets, e.g., the Fourier-based power spectrum density (PSD) [52] and 2-D MUSIC [53].

B. Unambiguous Range

For each target, the DOA and range information are respectively determined by ϕ_{θ_q} and ϕ_{R_q}, which are defined as the minimum phase difference in angle and range dimensions, respectively, i.e., the phase terms of $e^{-j\pi\sin(\theta_q)}$ and $e^{-j4\pi\Delta f R_q/c}$. In reality, however, phase observations are wrapped within $[-\pi,\pi)$. Therefore, the true phase can be expressed as

$$\phi_{\theta_q}^{(\text{true})} = \phi_{\theta_q} + 2m_{\theta_q}\pi, \tag{10}$$

$$\phi_{R_q}^{(\text{true})} = \phi_{R_q} + 2m_{R_q}\pi, \tag{11}$$

where m_{θ_q} and m_{R_q} are unknown integers. As a result, the range estimate is subject to range ambiguity [54], i.e.,

$$R_q = \frac{c\phi_{R_q}}{4\pi\Delta f} + \frac{cm_{R_q}}{2\Delta f}. \tag{12}$$

The latter term in (12) implies ambiguity in range due to phase wrapping. Thus, the range can be assumed as infinite values separated by $R_{\max} = c/(2\Delta f)$, which is referred to as the maximum unambiguous range. Therefore, the use of a large value of Δf will reduce the maximum unambiguous range. As a large frequency bandwidth is required to achieve proper range resolution, uniform frequency offsets must trade off between the range resolution and unambiguous range estimation. On other other hand, coprime frequency offsets allows the use of small Δf while collectively spanning a large signal bandwidth.

III. Frequency Diverse Coprime Arrays with Coprime Frequency Offsets

For the traditional FDA radar with N_t-element ULA and uniform frequency increment, it can localize up to $N_t^2 - 1$ targets, with a resolution $\mathcal{O}(1/N_t)$ in the angle and range domains, respectively. Compared with the uniform case, sparse arrays and sparse frequency offsets use the same number of sensors and frequencies to achieve a larger array aperture and frequency bandwidth. As a result, they improve the resolution and estimation accuracy. However, the number of resolvable targets using sparse arrays and sparse frequency offsets is still upper bounded by $N_t^2 - 1$, if those covariance matrix based approaches are used directly. Such the limitation can be overcome by the improvement of DOFs under the coarray equivalence.

A. Coarray Equivalence

By vectorizing the matrix $\mathbf{R}_{\mathbf{x}}$, we obtain the following $N_t^4 \times 1$ virtual measurement vector:

$$\mathbf{z} = \text{vec}(\mathbf{R}_{\mathbf{x}}) = \tilde{\mathbf{A}}_{p,f}\mathbf{b}_{p,f} + \sigma_n^2\tilde{\mathbf{i}}, \tag{13}$$

with

$$\tilde{\mathbf{A}}_{p,f} = [\tilde{\mathbf{a}}_{p,f}(\theta_1, R_1), \cdots, \tilde{\mathbf{a}}_{p,f}(\theta_Q, R_Q)], \tag{14}$$

$$\mathbf{b}_{p,f} = [\sigma_1^2, \cdots, \sigma_Q^2]^T, \tag{15}$$

$$\tilde{\mathbf{i}} = \text{vec}\left(\mathbf{I}_{N_t^2}\right), \tag{16}$$

where

$$\begin{aligned}\tilde{\mathbf{a}}_{p,f}(\theta_q, R_q) &= \mathbf{a}_{p,f}^*(\theta_q, R_q) \otimes \mathbf{a}_{p,f}(\theta_q, R_q) \\ &= \mathbf{a}_p^*(\theta_q) \otimes \mathbf{a}_f^*(R_q) \otimes \mathbf{a}_p(\theta_q) \otimes \mathbf{a}_f(R_q) \\ &= (\mathbf{a}_p^*(\theta_q) \otimes \mathbf{a}_p(\theta_q)) \otimes (\mathbf{a}_f^*(R_q) \otimes \mathbf{a}_f(R_q)) \\ &= \tilde{\mathbf{a}}_p(\theta_q) \otimes \tilde{\mathbf{a}}_f(R_q)\end{aligned} \tag{17}$$

for $1 \le q \le Q$. Benefiting from the Vandermonde structure of $\mathbf{a}_p(\theta_q)$ and $\mathbf{a}_f(R_q)$, the entries in $\tilde{\mathbf{a}}_p(\theta_q)$ and $\tilde{\mathbf{a}}_f(R_q)$ are still in the forms of $e^{-j\pi(p_i-p_j)\sin(\theta_q)}$ and $e^{-j4\pi(\xi_i-\xi_j)\Delta f R_q/c}$, for $i,j = 1,\cdots,N_t$. As such, we can regard $\mathbf{z}$ as a received signal vector from a single-snapshot signal vector $\mathbf{b}_{p,f}$, and the matrix $\tilde{\mathbf{A}}_{p,f}$ corresponds to the virtual array sensors and virtual frequency offsets which are respectively located at the sensor-lags between all sensor pairs and frequency-offsets between all frequency pairs. The targets can thus be localized by using the space-frequency coarray, in lieu of the original antennas and frequencies. Note that the number of elements in the space-frequency coarray structure are directly determined by the distinct values of $(p_i - p_j)$ and $(\xi_i - \xi_j)$ for $i,j = 1,\cdots,N_t$. Non-uniform arrays can substantially increase the number of DOFs by reducing the number of redundant elements in the coarray. In other words, the number of DOFs would be reduced if different pairs of sensors or frequency offsets yield same lags when the uniform arrays are exploited.

B. Coprime Arrays with Coprime Frequency Offsets

Among the different choices that are available for sparse array and frequency offset designs, the recently proposed coprime configurations [27] offer a systematical design capability and DOF analysis involving sensors, samples, or frequencies. In this paper, we use the extended coprime structure which is proposed in [55] as an example. Extensions to other generalized coprime structures that achieve higher DOFs are straightforward [34].

As shown in Fig. 2, the extended coprime array structure utilizes a coprime pair of uniform integers. The coprime array consists of a $2M$-sensor uniform linear subsarray with an

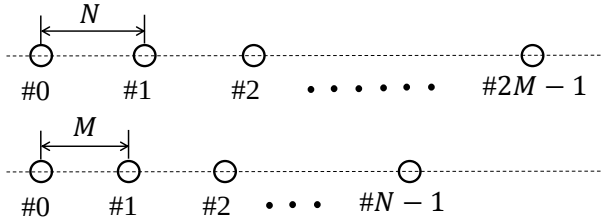

Fig. 2. The extended coprime structure.

interelement spacing of N, and an N-sensor uniform linear subarray with an interelement spacing of M. The two integers M and N are chosen to be coprime, i.e., their greatest common divisor is one. In addition, $M < N$ is assumed. Define

$$\mathbb{P}_{(M,N)} = \{Mn | 0 \leq n \leq N-1\} \bigcup \{Nm | 0 \leq m \leq 2M-1\} \tag{18}$$

as the union of two sparsely sampled integer subsets with respect to the pair of coprime integers (M, N). As such, the yielding correlation terms have the positions

$$\mathbb{L}_{(M,N)} = \{\pm(Mn - Nm) | 0 \leq m \leq 2M-1, 0 \leq n \leq N-1\}. \tag{19}$$

An example is illustrated in Fig. 3, where $M = 2$ and $N = 3$. Fig. 3(a) shows the physical elements of extended coprime structure, and the positions of the corresponding correlation terms are depicted in Fig. 3(b). Notice that "holes", e.g., ± 8 in this case, still exist in the virtual domain and are indicated by $\times$ in the figure. It is proved in [56] that $\mathbb{L}_{(M,N)}$ can achieve at least MN (up to $(3MN + M - N + 1)/2$) DOFs with only $2M + N - 1$ (two subsets share the first element) entries in $\mathbb{P}_{(M,N)}$.

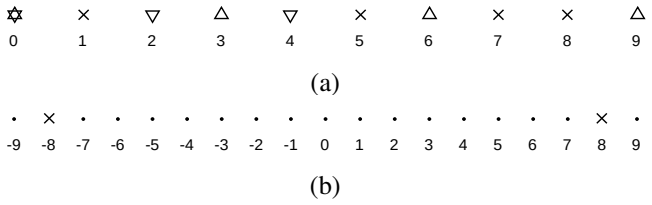

Fig. 3. An example for the extended coprime structure. (a) The physical elements in $\mathbb{P}_{(M,N)}$ ($\triangle$: Subset 1; ∇: Subset 2); (b) The corresponding correlation term positions in $\mathbb{L}_{(M,N)}$.

When coprime arrays and coprime frequency offsets with pairs of coprime integers (M, N) is exploited, there are at least MN available DOFs in each $\mathbf{a}_p(\theta_q)$ and $\mathbf{a}_f(R_q)$. That is, the resulting virtual array elements and virtual frequency offsets enable estimation of at least MN distinct DOAs and MN distinct ranges of targets. Benefitting from the sparse structure, the proposed coprime array with coprime frequency offsets offers a larger aperture and frequency span, thus resulting in an improved resolution in both angular and range domains. Further, it has less redundant entries in the covariance matrix $\mathbf{R}_{\mathbf{x}}$, implying that the resulting coarray structure and frequency lag sets provide a higher number of DOFs that can be used to identify more targets using the CS based methods.

The localization problem in (13) is similar to handling multiple targets that are fully coherent. In this case, the covariance matrix constructed from the virtual signal vector is rank-1 and, as a result, subspace-based localization approaches fail to function. A well-known approach that restores the rank of the covariance matrix is spatial smoothing [57], [58]. A major disadvantage of such approach is that only consecutive lags in the virtual observations can be used so that every subarray has a similar manifold (e.g., $[-7, 7]$ in Fig. 3(b)), whereas the virtual sensors that are separated by any holes have to be discarded. Alternatively, this problem can be solved by using sparse reconstruction methods (e.g., [34], [59]) which, by taking advantages of the fact that the targets are sparse in the angle-range domain, utilize all consecutive and non-consecutive lags (e.g., ± 9 and $[-7, 7]$ in Fig. 3(b)) in the coarray so as to fully utilize the available DOFs offered by the coarray configurations.

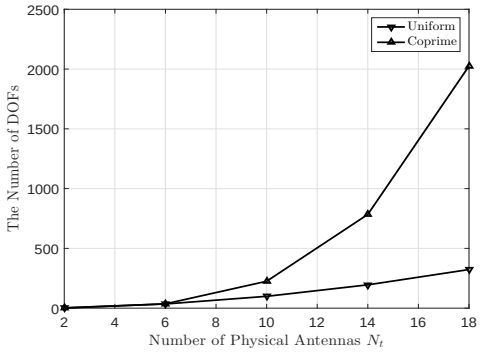

Fig. 4. The number of DOFs versus N_t.

Provided that sufficient snapshots are available for reliable covariance matrix estimation, at least $\mathcal{O}(MN)$ targets (no same DOA and no same range), up to $\mathcal{O}(M^2N^2)$ targets (each of MN DOAs has MN distinct ranges), can thus be localized by using $N_t = 2M + N - 1$ antennas and $N_t = 2M + N - 1$ frequencies. For a given number of N_t, the maximum number of DOFs can be further optimized by

$$\begin{aligned} \text{Maximize} \quad & M^2N^2 \\ \text{subject to} \quad & 2M + N - 1 = N_t, \\ & M < N, \quad M, N \in \mathbb{N}^+. \end{aligned} \tag{20}$$

It is demonstrated in [31] that the valid optimal coprime pair to maximize MN is the one that has $2M$ and N as close as possible. This is satisfied by choosing $N = 2M - 1$. In this case, more than $\left[N_t^2(N_t + 2)^2\right]/64$ DOFs can be obtained. Therefore, the frequency diverse coprime arrays with coprime frequencies can resolve more targets than that of conventional FDA with ULA and uniform frequency increment (i.e., $N_t^2 - 1$) when $N_t \geq 6$, as shown in Fig. 4.

IV. Target localization using multitask BCS

In the following, we perform multi-target localization in the sparse reconstruction framework. The general focus of proposed methods is to resolve a higher number of targets and improve the localization accuracy by fully utilizing all the virtual observations achieved from lags in both sensor positions and frequencies. For the simplicity and clarity of the presentation, we assume the targets to be placed on a predefined grid. Direct application of the proposed method in the presence of dictionary mismatch would yield performance degradation. However, various techniques, such as those cited in [32], [33], [60], [61], can be used to overcome this problem by exploring the joint sparsity between signals and the grid mismatch variables.

The virtual signal vector $\mathbf{z}$ in (13) can be sparsely represented over the entire discretized angular grids as

$$\mathbf{z} = \mathbf{\Phi}\mathbf{b} + \boldsymbol{\epsilon}, \tag{21}$$

where $\mathbf{\Phi} = \left[\mathbf{\Phi}_s, \tilde{\mathbf{i}}\right]$. Herein, $\mathbf{\Phi}_s$ is defined as the collection of steering vectors $\tilde{\mathbf{a}}_{p,f}(\theta_{g_1}, R_{g_2})$ over all possible grids θ_{g_1} and R_{g_2}, $g_1 = 1, \ldots, G_1, g_2 = 1, \ldots, G_2$, with $G = G_1 G_2 \gg N_t^4 > Q$, and $\mathbf{b}_s$ is the sparse vector whose non-zero entry positions correspond to the DOAs and ranges of the targets, i.e., $(\theta_q, R_q), q = 1, \ldots, Q$. The term $\tilde{\mathbf{i}}$ in the dictionary accounts for noise variance terms that have unequal values in the vectorized entries. In addition, an error vector ϵ is included to represent the discrepancies between the statistical expectation and the sample average in computing the covariance matrix $\mathbf{R}$. The discrepancies are modelled as i.i.d. complex Gaussian as a result of a sufficiently large number of samples employed in the averaging.

In this paper, we elect to perform the sparse signal reconstruction within the BCS framework [45]–[51] stemming from their superior performance and robustness to dictionary coherence. In particular, the complex multitask BCS approach developed in [45] is used to deal with all the sparse reconstruction problems. Thus, the following sparse Bayesian model is presented as an MMV model with P tasks (measurements), whereas the SMV problem in (21) can be considered as a special case with a single task, i.e., $P = 1$.

A. Sparse Bayesian Formulation

The MMV model is expressed as

$$\mathbf{Z} = \mathbf{\Phi}\mathbf{B}, \tag{22}$$

where $\mathbf{Z} = [\mathbf{z}_1, \cdots, \mathbf{z}_P]$ and $\mathbf{B} = [\mathbf{b}_1, \cdots, \mathbf{b}_P]$. The matrix $\mathbf{B}$ is jointly sparse (or row sparse), i.e., all columns of $\mathbf{B}$ are spares and share the same support.

Assume that the entries in jointly sparse matrix $\mathbf{B}$ are drawn from the product of the following zero-mean complex Gaussian distributions:

$$\Pr(\mathbf{B}|\boldsymbol{\alpha}) = \prod_{p=1}^{P} \mathcal{CN}(\mathbf{b}_p|\mathbf{0}, \mathbf{\Lambda}), \tag{23}$$

where $\boldsymbol{\alpha} = [\alpha_1, \ldots, \alpha_G]^T$ and $\mathbf{\Lambda} = \mathrm{diag}(\boldsymbol{\alpha})$. It is noted that the gth row of $\mathbf{B}$ trends to be zero when $\alpha_g, g = 1, \cdots, G$ is set to zero [46]. In addition, $\boldsymbol{\alpha}$ is placed on a complex variable directly. As such, it achieves improved sparse signal reconstruction because by utilizing the group sparsity of the real and imaginary components than the methods that simply decomposing them into independent real and imaginary components.

To encourage the sparsity, a Gamma prior is placed on α_g, which is conjugate to the Gaussian distribution,

$$\alpha_g \sim \Gamma(\alpha_g|1, \rho), g \in [1, \cdots, G], \tag{24}$$

where $\rho \in \mathbb{R}^+$ is a fixed priori. It has been demonstrated in [62] that a proper choice of ρ encourages a sparse representation for the coefficients. Then, we have

$$\Pr(\boldsymbol{\alpha}|a, b) = \prod_{g=1}^{G} \Gamma(\alpha_g|1, \rho). \tag{25}$$

All columns of $\mathbf{B}$ share the same prior due to the group sparse property. Base on [63], both of the real and image parts of $\mathbf{b}_p$, $p = 1, \cdots, P$, are Laplace distributed and share the same pdf that is strongly peaked at the origin. As such, this two-stage hierarchical prior is a sparse prior that favors most rows of $\mathbf{B}$ being zeros.

A Gaussian prior $\mathcal{CN}(\mathbf{0}, \beta_0^{-1}\mathbf{I}_2)$ is also placed on the error vector $\boldsymbol{\epsilon}$. Then, we have,

$$\Pr(\mathbf{Z}|\mathbf{B}, \beta_0) = \prod_{p=1}^{P} \mathcal{CN}(\mathbf{z}_p|\mathbf{\Phi}\mathbf{b}_p, \beta_0^{-1}\mathbf{I}), \tag{26}$$

Likewise, the Gamma prior is placed on β_0 with hyperparameters c and d, expressed as

$$\Pr(\beta_0|c, d) = \Gamma(\beta_0^{-1}|c, d), \tag{27}$$

where $\mathrm{Gamma}(\beta_0^{-1}|a, b) = \Gamma(a)^{-1} b^a \beta_0^{-(a-1)} e^{-\frac{b}{\beta_0}}$.

By combining the stages of the hierarchical Bayesian model, the joint pdf becomes

$$\Pr(\mathbf{Z}, \mathbf{B}, \boldsymbol{\alpha}, \beta_0) = \Pr(\mathbf{Z}|\mathbf{B}, \beta_0)\Pr(\mathbf{B}|\boldsymbol{\alpha})\Pr(\boldsymbol{\alpha}|1, \rho)\Pr(\beta_0|c, d). \tag{28}$$

To make this Gamma prior non-information, we set $c = d = 0$ in this paper as in [46]–[51].

B. Bayesian Inference

Assuming $\boldsymbol{\alpha}$ and β_0 are known, given the measurement $\mathbf{Z}$ and the corresponding dictionary $\mathbf{\Phi}$, the posterior for $\mathbf{B}$ can be obtained analytically using Bayes's rule, expressed as a Gaussian distribution with mean $\boldsymbol{\mu}$ and variance $\mathbf{\Sigma}$

$$\Pr(\mathbf{B}|\mathbf{Z}, \boldsymbol{\alpha}, \beta_0) = \prod_{p=1}^{P} \mathcal{CN}(\mathbf{b}_p|\boldsymbol{\mu}_p, \mathbf{\Sigma}), \tag{29}$$

where

$$\boldsymbol{\mu}_p = \beta_0^{-1}\mathbf{\Sigma}\mathbf{\Phi}^H\mathbf{z}_p, \tag{30}$$

$$\mathbf{\Sigma} = \left[\beta_0^{-1}\mathbf{\Phi}^H\mathbf{\Phi} + \mathbf{F}^{-1}\right]^{-1}. \tag{31}$$

The associated learning problem, in the context of relevance vector machine (RVM), thus becomes the search for the $\boldsymbol{\alpha}$ and β_0. In RVM, the values of $\boldsymbol{\alpha}$ and β_0 are estimated from the data by performing a type-II maximum likelihood (ML) procedure [62]. Specially, by marginalizing over the $\mathbf{B}$, the marginal likelihood for $\boldsymbol{\alpha}$ and β_0, or equivalently, its logarithm $\mathcal{L}(\boldsymbol{\alpha}, \beta_0)$ can be expressed analytically as

$$\begin{aligned}\mathcal{L}(\boldsymbol{\alpha}, \beta_0) &= \sum_{p=1}^{P} \log \Pr(\mathbf{b}_p|\boldsymbol{\alpha}, \beta_0) \\ &= \sum_{p=1}^{P} \log \int \Pr(\mathbf{z}_p|\mathbf{b}_p, \beta_0)\Pr(\mathbf{b}_p|\boldsymbol{\alpha})d\mathbf{b}_p \\ &= \mathrm{const} - \frac{1}{2}\sum_{p=1}^{P} \log |\mathbf{C}| + (\mathbf{z}_p)^H \mathbf{C}^{-1}\mathbf{z}_p \end{aligned} \tag{32}$$

with

$$\mathbf{C} = \beta_0\mathbf{I} + \mathbf{\Phi}\mathbf{F}\mathbf{\Phi}^H. \tag{33}$$

Denote $\boldsymbol{U} = [\boldsymbol{\mu}_1, \cdots, \boldsymbol{\mu}_P] = \beta_0^{-1}\mathbf{\Sigma}\mathbf{\Phi}^H\mathbf{Z}$, $\underline{\mathbf{B}} = \mathbf{B}/\sqrt{P}$, $\underline{\mathbf{Z}} = \mathbf{Z}/\sqrt{P}$, $\underline{\boldsymbol{U}} = \boldsymbol{U}/\sqrt{P}$, and $\underline{\rho} = \rho/P$. An ML approximation employs the point estimates for $\boldsymbol{\alpha}$ and β_0 to maximize (32),

which can be implemented via the expectation maximization (EM) algorithm to yield

$$\alpha_g^{(\text{new})} = \frac{\sqrt{1+4\underline{\rho}(\|\underline{\boldsymbol{\mu}}^g\|_2^2+\Sigma_{g,g})}-1}{2\underline{\rho}}, \quad g\in[1,\cdots,G], \tag{34}$$

$$\beta_0^{(\text{new})} = \frac{\mathrm{E}\{\|\underline{\mathbf{Z}}-\boldsymbol{\Phi}\underline{\mathbf{B}}\|_F^2\}}{N_{\boldsymbol{\Phi}}}, \tag{35}$$

where $\underline{\boldsymbol{\mu}}^g$ is the gth row of matrix $\underline{\boldsymbol{U}}$ and $\Sigma_{g,g}$ is the (g,g)th entry of matrix $\boldsymbol{\Sigma}$. In addition, $N_{\boldsymbol{\Phi}}$ is the number of rows of $\boldsymbol{\Phi}$.

It is noted that, because $\boldsymbol{\alpha}^{(\text{new})}$ and $\beta_0^{(\text{new})}$ are a function of $\boldsymbol{\mu}_p$ and $\boldsymbol{\Sigma}$, while $\boldsymbol{\mu}_p$ and $\boldsymbol{\Sigma}$ are a function of $\boldsymbol{\alpha}$ and β_0, this suggests an iterative algorithm that iterates between (30)–(31) and (34)–(35), until a convergence criterion is satisfied or the maximum number of iterations is reached. In each iteration, the computational complexity is $\mathcal{O}(\max(N_{\boldsymbol{\Phi}}G^2, N_{\boldsymbol{\Phi}}GP))$ with an $N_{\boldsymbol{\Phi}}\times G$ dictionary $\boldsymbol{\Phi}$ [48].

C. Complexity Analysis

For the case of 2-D BCS, the corresponding joint angle-range of targets, $(\hat{\theta}_q,\hat{R}_q)$, $q=1,\cdots,Q$, can be estimated by positions of the nonzero entries in $\mathbf{b}$ in (21). In the sequel, we analyze its computational complexity, which can be divided into the following three stages:

S1: Compute the $N_t^2\times N_t^2$ covariance matrix $\hat{\mathbf{R}}_{\text{x}}$ with (9).
S2: Generate the $N_t^4\times 1$ virtual array data $\mathbf{z}$ with (13) by vectorizing the covariance matrix.
S3: Perform target localization to obtain $(\hat{\theta}_q,\hat{R}_q)$, $q=1,\cdots,Q$ using (30)–(31) and (34)–(35), based on the BCS ($P=1$) with an $N_t^4\times G_1G_2$ dictionary.

In *S1*, there are $\mathcal{O}(N_t^4T)$ complex multiplications, whereas no multiplication operation is needed for vectorization in *S2*. For the BCS, we might need $\mathcal{O}(\kappa N_t^4G_1^2G_2^2)$ complex multiplication operations, where κ is the number of iterations. Therefore, the total computational load, i.e., $\mathcal{O}(N_t^4T+\kappa N_t^4G_1^2G_2^2)$, is very huge because the exhaustive 2-D searching process, which motivates the development of fast algorithms.

V. A Fast Algorithm for Target Localization

In this section, we develop an algorithm based on the multitask BCS, wherein the 2-D sparse reconstruction problem is cast as separate 1-D sparse reconstruction problems. Therefore, the computational complexity can be reduced.

Stacking $x_{k,l}(t)$ for all $l=1,...,N_t$ yields the following $N_t\times 1$ vector,

$$\mathbf{x}_k(t)=\sum_{q=1}^{Q}\rho_q(t)e^{-j\frac{4\pi f_k}{c}R_q}\mathbf{a}_p(\theta_q)+\mathbf{n}_k(t). \tag{36}$$

As such, the vector $\mathbf{x}_k(t)$ behaves as the received signal of the array, corresponding to the frequency f_k, $k=1,\cdots,N_t$.

The cross-covariance matrix between data vectors $\mathbf{x}_k(t)$ and $\mathbf{x}_{k'}(t)$, respectively corresponding to frequencies f_k and $f_{k'}$, $1\le k,k'\le N_t$, is obtained as

$$\mathbf{R}_{\mathbf{x}_{kk'}}=\mathrm{E}[\mathbf{x}_k(t)\mathbf{x}_{k'}^H(t)]=\sum_{q=1}^{Q}\sigma_q^2e^{-j\frac{4\pi\Delta f_{kk'}}{c}R_q}\mathbf{a}_p(\theta_q)\mathbf{a}_p^H(\theta_q), \tag{37}$$

where $\Delta f_{kk'}=f_k-f_{k'}=(\xi_k-\xi_{k'})\Delta f$. Note that the dimension of $\mathbf{R}_{\mathbf{x}_{kk'}}$ is reduced to $N_t\times N_t$, compared to the $N_t^2\times N_t^2$ matrix $\mathbf{R}_{\text{x}}$ in (8). In practice, the cross-covariance matrix is estimated by using T available samples, i.e.,

$$\hat{\mathbf{R}}_{\mathbf{x}_{kk'}}=\frac{1}{T}\sum_{t=1}^{T}\mathbf{x}_k(t)\mathbf{x}_{k'}^H(t), 1\le k,k'\le N_t. \tag{38}$$

Vectorizing this matrix yields the following $N_t^2\times 1$ vector

$$\mathbf{z}_{kk'}=\mathrm{vec}(\mathbf{R}_{\mathbf{x}_{kk'}})=\bar{\mathbf{A}}\mathbf{b}_{f_{kk'}}, \tag{39}$$

where

$$\bar{\mathbf{A}}=[\tilde{\mathbf{a}}_p(\theta_1),\cdots,\tilde{\mathbf{a}}_p(\theta_Q)], \tag{40}$$

$$\mathbf{b}_{f_{kk'}}=[\sigma_1^2e^{-j\frac{4\pi\Delta f_{kk'}}{c}R_1},\cdots,\sigma_Q^2e^{-j\frac{4\pi\Delta f_{kk'}}{c}R_Q}]^T. \tag{41}$$

Similarly, (39) can be sparsely represented over the entire angular grids as

$$\mathbf{z}_{kk'}=\bar{\boldsymbol{\Phi}}\bar{\mathbf{b}}_{kk'}, \tag{42}$$

where the $N_t^2\times G_1$ dictionary $\bar{\boldsymbol{\Phi}}$ is defined as the collection of steering vectors $\tilde{\mathbf{a}}_p(\theta_g)$ over all possible grids θ_{g_1}, $g_1=1,\ldots,G_1$, with $G_1\gg Q$. As such, the DOAs θ_q, $q=1,\cdots,Q$, are indicated by the nonzero entries in the sparse vector $\bar{\mathbf{b}}_{kk'}$, whose values describe the corresponding coefficients $\sigma_q^2e^{-j\frac{4\pi(\xi_k-\xi_{k'})\Delta f}{c}R_q}$. Note that the nonzero entries corresponding to different frequency pairs share the same positions as they are associated with the same DOAs of the Q targets. However, their values differ for each frequency pair. Therefore, $\mathbf{z}_{kk'}$ exhibits a group sparsity across all frequency pairs and the problem described in (42) can be solved in the MMV sparse reconstruction context.

Denote $\mathbf{Z}=[\mathbf{z}_1,\cdots,\mathbf{z}_P]$ as the collection of vectors $\mathbf{z}_{kk'}$, corresponding to all $P=N_t^2$ frequency pairs. Then, the MMV sparse reconstruction problem is expressed as

$$\mathbf{Z}=\bar{\boldsymbol{\Phi}}\bar{\mathbf{B}}, \tag{43}$$

where $\mathbf{B}=[\bar{\mathbf{b}}_1,\cdots,\bar{\mathbf{b}}_P]$ is the sparse matrix that can be reconstructed by the multitask BCS.

Denote $\bar{Q}$ as the number of distinct DOAs of Q targets, the $n_{\bar{q}}$, as the index of those nonzero positions in $\bar{\mathbf{B}}$ corresponding to $\theta_{\bar{q}}$, $\bar{q}=1,\cdots,\bar{Q}$. In addition, the $P\times 1$ vector $\mathbf{b}_{n_{\bar{q}}}$ is denoted as the $n_{\bar{q}}$th column of $\bar{\mathbf{B}}^T$. Then, the range can be estimated by solving the following sparse reconstruction problem:

$$\mathbf{b}_{n_{\bar{q}}}=\boldsymbol{\Psi}\mathbf{R}_{n_{\bar{q}}}, \quad \bar{q}=1,\cdots,\bar{Q}, \tag{44}$$

where $\boldsymbol{\Psi}$ is the $N_t^2\times G_2$ dictionary, whose g_2th column, $g_2=1,\ldots,G_2$, is

$$\boldsymbol{\Psi}_{g_2}=\left[1,\cdots,e^{-j\frac{4\pi(\xi_k-\xi_{k'})}{c}R_{g_2}},\cdots,1\right]^T, \tag{45}$$

with $1 \le k, k' \le N_t$. Then, the range on $\theta_{\bar{q}}$, $\bar{q} = 1, \cdots, \bar{Q}$ can be indicated by positions of nonzero entries in sparse vector $\mathbf{R}_{n_{\bar{q}}}$.

As a summary, the proposed approach can be divided into the following four stages:

S1: Compute all $N_t \times N_t$ covariance matrix $\hat{\mathbf{R}}_{\mathbf{x}_{kk'}}$ using (38), $1 \le k, k' \le N_t$.

S2: Generate all the $N_t^2 \times 1$ virtual array data $\mathbf{z}_{kk'}$ with (39) by vectorizing the covariance matrix, $1 \le k, k' \le N_t$.

S3: Perform DOA estimation of the targets, based on the multitask sparse reconstruction $\left(P = N_t^2\right)$ model in (43) with an $N_t^2 \times G_1$ dictionary.

S4: Perform range estimation of the targets, based on the sparse reconstruction model in (44) with an $N_t^2 \times G_2$ dictionary.

In *S1*, there are $\mathcal{O}(N_t^4 T)$ multiplication operations. The complexity in *S3* and *S4* is $\mathcal{O}(\kappa_1 N_t^2 G_1^2)$ and $\mathcal{O}(\kappa_2 N_t^2 G_2^2)$, respectively, where κ_1 and κ_2 are the corresponding number of iterations. Thus, the total computation load is $\mathcal{O}\left(N_t^4 T + \kappa_1 N_t^2 G_1^2 + \kappa_2 \bar{Q} N_t^2 G_2^2\right)$, which is much lower than $\mathcal{O}(N_t^4 T + \kappa N_t^4 G_1^2 G_2^2)$ in Section IV.

Remarks: The following observations can be made regarding the relationship between the joint and the two-step estimation methods:

(1) Both estimation methods achieve the same number of DOFs from the coarray;

(2) The two-step estimation method requires a significantly reduced complexity. However, the corresponding performance becomes sub-optimal due to error propagation. i.e., errors in the DOA estimation stage may yield additional perturbations in the range estimation.

VI. Simulation Results

For illustrative purposes, we consider an FDA radar exploiting coprime array and coprime frequency offset, where $M = 2$ and $N = 3$ are assumed. The extended coprime structure consist of $N_t = (2M + N - 1) = 6$ physical elements, and has $(3MN + M - N + 1)/2 = 9$ DOFs in the virtual domain. As such, the increased number of DOFs enables to localize more than $M^2 N^2 = 36$ targets with only 6 antennas exploiting 6 frequencies.

The unit interelement spacing is $d = \lambda_0/2$, where λ_0 is the wavelength with respect to the carrier frequency $f_0 = 1$ GHz. We choose the unit frequency increment to be $\Delta f = 30$ KHz, resulting maximum unambiguous range $R_{\max} = c/(2\Delta f) = 5000$ m. In all simulations, Q far-field targets with identical target scattering powers are considered. The qth target is assumed to be on angle-range plane (θ_q, R_q), where $\theta_q \in [-60^\circ, 60^\circ]$ and $R_q \in [1000, 5000]$ m, for $q = 1, \cdots, Q$. The localization performance for the coprime array and coprime frequency offset (CA-CFO) is examined in terms of the resolution, accuracy, and the maximum number of resolvable targets. The average root mean square error (RMSE) of the estimated DOAs and ranges, expressed as

$$\mathrm{RMSE}_\theta = \sqrt{\frac{1}{IQ}\sum_{i=1}^{I}\sum_{q=1}^{Q}(\hat{\theta}_q(i) - \theta_q)^2},$$
$$\mathrm{RMSE}_R = \sqrt{\frac{1}{IQ}\sum_{i=1}^{I}\sum_{q=1}^{Q}(\hat{R}_q(i) - R_q)^2}, \qquad (46)$$

are used as the metric for estimation accuracy, where $\hat{\theta}_q(i)$ and $\hat{R}_q(i)$ are the estimates of θ_q and R_q for the ith Monte Carlo trial, $i = 1, \ldots, I$. We use $I = 500$ independent trials in simulations.

A. Joint Estimation Method versus Two-step Estimation Method

We first compare the performance of the joint estimation method and two-step estimation method. $Q = 1$ target with $(10^\circ, 1000\mathrm{m})$ is considered. The dictionary matrices $\bar{\mathbf{\Phi}}$ and $\mathbf{\Psi}$ are assumed to contain all possible grid entries within $(5^\circ, 15^\circ)$ and $(1250\ \mathrm{m}, 1350\ \mathrm{m})$ with uniform intervals $\theta_{g_1} = 0.2^\circ$ and $R_{g_2} = 1$ m, respectively. Fig. 5 compares the RMSE performance of DOA and range estimations with respect to the input signal-to-noise ratio (SNR), where 500 snapshots are used. In Fig. 6, we compare the RMSE performance with respect to the number of snapshots, where the input SNR is set to -5 dB. It is clear that the joint estimation method achieves slightly better estimation accuracy at the cost of much higher computation complexity.

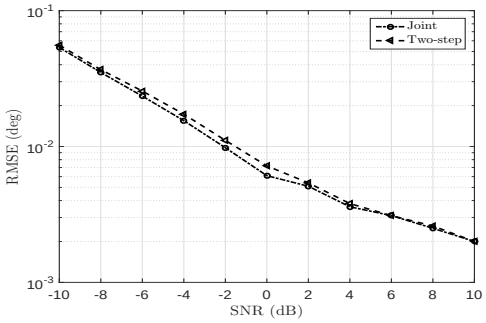

(a)

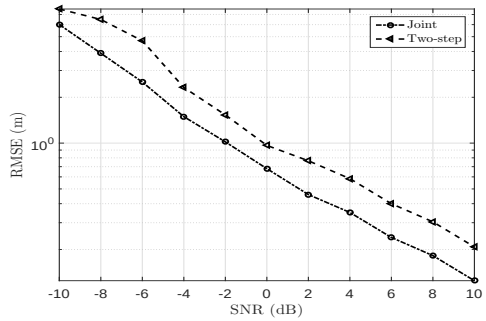

(b)

Fig. 5. RMSE versus SNR using the joint and two-step estimation methods ($Q = 1$ and $T = 500$). (a) RMSE_θ; (b) RMSE_R

B. CA-CFO versus Other Array Configuration and Frequency Offset Designs

Next, we examine the localization performance for different array configuration and frequency offset designs. Particularly, the proposed CA-CFO is compared with uniform linear array and uniform frequency offset (ULA-UFO). Uniform linear array with coprime frequency offset (ULA-CFO), and coprime array and uniform frequency offset (CA-UFO) are also considered. In order to reduce the computational load, we use the fast algorithm in section V for target localization in simulations.

In Fig. 7, we compare the resolution performance of different schemes. $Q = 8$ targets whose true positions are shown in Fig. 7(a) are considered. The dictionary matrices $\bar{\mathbf{\Phi}}$ and $\mathbf{\Psi}$ contain steering vectors over all possible grids in $(-60^\circ, 60^\circ)$ and $(1000\ \mathrm{m}, 5000\ \mathrm{m})$ with uniform intervals $\theta_{g_1} = 1^\circ$ and $R_{g_2} = 100\ \mathrm{m}$, respectively. Note that the number of targets is larger than the number of antennas, and the traditional phased array radar does not have sufficient DOFs to resolve all targets. The covariance matrix are obtained by using 500 snapshots in the presence of noise with a 0 dB SNR, and the corresponding localization performance are illustrated in Figs. 7(b)–(e). It is evident that only the case of CA-CFO can identify targets correctly because the increased DOFs in both virtual array and frequency can estimate more DOAs than the number of antennas, and more ranges than the number of frequencies. In addition, the corresponding larger apertures in both angle and range domains enable the CA-CFO case to resolve the closely spaced targets. The conventional FDA with ULA-UFO fails to separate both pairs of the targets with closely spaced angle and closely spaced range. However, the scenario of CA-UFO can resolve the pair of targets with closely spaced angle and the ULA-CFO case can identify targets with closely spaced range, benefitting from the increased DOFs in the angle and range domains, respectively.

We further compare the estimation accuracy through Monte Carlo simulations. To proceed with the comparison, we consider $Q = 2$ targets with $(10^\circ, 1300\ \mathrm{m})$ and $(25^\circ, 1700\mathrm{m})$, which can be separated for all cases. The dictionary matrices $\bar{\mathbf{\Phi}}$ and $\mathbf{\Psi}$ are assumed to contain entries corresponding to all possible grids in $(10^\circ, 30^\circ)$ and $(1000\ \mathrm{m}, 2000\ \mathrm{m})$ with uniform intervals $\theta_{g_1} = 0.2^\circ$ and $R_{g_2} = 10\ \mathrm{m}$, respectively. Fig. 8 compares the RMSE performance of DOA and range estimations with respect to the input SNR for different array configurations and frequency offset structures, where 500 snapshots are used. In Fig. 9, we compare the RMSE performance with respect to the number of snapshots, where the input SNR is set to -5 dB. It is evident that the accuracy of both DOA and range estimates is improved as the SNR and the number of snapshots increase. In comparison with the uniform array/offset case, the coprime array/offset structure benefits from more independent measurements under the CS framework. It is shown that the CA-UFO and ULA-CFO respectively achieve improved estimation accuracy in the angular and range domains than that of the ULA-UFO owing to the coprime structure in the sensor positions and frequency offsets. In particular, the CA-CFO achieves the best performance as the advantages of coprime structure are presented in both angular and range domains.

In Fig. 10, we consider $Q = 56$ targets. Note that this number is more than the available DOFs obtained from the cases of ULA-UFO (the conventional FDA radar), ULA-CFO, and CA-UFO. As the virtual array and virtual frequency offset are obtained from the estimated covariance matrix based on the received data samples, the virtual steering matrix is sensitive to the noise contamination. To clearly demonstrate the sufficient DOFs for localization of a large number of targets, we use 2000 snapshots in presence of noise with a 10 dB input SNR. It is evident that all 56 signals can be identified correctly, which demonstrates the effectiveness of the CA-CFO in resolving more targets.

C. Sparsity-based Method versus Subspace-based Method

In Figs. 11–13, we compare the sparsity-based method and the MUSIC algorithm with spatial smoothing (MUSIC-SS) applied to the CA-CFO configuration. Note that the spatial smoothing technique is applied to the covariance matrix of the virtual measurement vector $\mathbf{z}$ so that its rank can be restored before the MUSIC algorithm is applied. In this case, only consecutive lags, i.e., $[-7, 7]$, can be used so that every submatrix has a similar manifold. The corresponding number of available DOFs is less than that of the proposed sparsity-based approach, which utilizes all unique lags [34]. In Fig. 11, we examine their resolution for $Q = 5$ closely spaced targets, whose true positions are shown in Fig. 11(a). The localization results, depicted in Figs. 11(b) and 11(c), are obtained by using 500 snapshots with a 0 dB SNR. It is clear that the sparsity-based method outperforms the MUSIC-SS approach for resolving the closely spaced targets, since it exploits all distinct lags to form a virtual space-frequency structure, thus yielding a larger array aperture and frequency span compared to the corresponding MUSIC-SS technique which only uses consecutive lags. The respective RMSE performance is compared in Figs. 12 and 13 under the same target scenario considered in Figs. 8 and 9, whereas $Q = 2$ targets located at $(10^\circ, 1300\ \mathrm{m})$ and $(25^\circ, 1700\ \mathrm{m})$ are present. In Fig. 12, 500 snapshots are used, while a -5 dB SNR is assumed in Fig. 13. It is evident that the proposed sparsity-based method achieves a lower RMSE than the MUSIC-SS due to the higher number DOFs in both angular and range domains. This simulation example shows that the sparsity-based method achieves better performance than the MUSIC-SS counterparts do.

D. Proposed Method versus Existing Methods

In Figs. 14–16, we compare the performance of the proposed method with the existing methods using sparse arrays. The methods in [42] and [43], which are referred to as the Nested-MUSIC and Nested-CS, respectively, employ a nested array configuration but with the uniform time-delayer and frequency increment. As a consequence, it has only $\mathcal{O}(N_t)$ frequency DOFs with a smaller spectral span for a coarse range resolution, although it has the same $\mathcal{O}(N_t^2)$ spatial DOFs as the proposed coprime FDA radar configuration.

The same target scenario considered in Figs. 11–13 is used for performance comparison. Fig. 14 depicts the angle-range resolution, wherein the true positions and results obtained from the proposed method are reproduced from Fig. 11(a) and Fig. 11(c) as Fig. 14(a) and Fig. 14(b) for the convenience of comparison. The corresponding results using the Nested-MUSIC and Nested-CS methods are presented in Figs. 14(c) and 14(d), respectively. It is evident that only the proposed method can resolve these closely spaced targets in the range. Furthermore, the Nested-MUSIC method produces more blurry spectra than the Nested-CS for targets with a small angulare separation. The RMSE is compared in Figs. 15 and 16. It is clear that the Nested-MUSIC and Nested-CS methods suffer from significant performance degradation in the range domain due to the reduced spectral span and range-domain DOFs. Accordingly, the Nested-CS outperforms the Nested-MUSIC owing to its utilizations of all distinct lags in the coarray structure.

VII. Conclusions

In this paper, we proposed a novel sparsity-based multi-target localization algorithm, which incorporates both coprime arrays and coprime frequency offsets in an FDA radar platform. By exploiting the sensor position lags and frequency differences, the proposed technique achieved a high number of DOFs representing a larger array aperture and increased frequency increments compared to conventional approaches. These attributes enable high-resolution target localization of significantly more targets than the number of physical sensors. A fast algorithm was developed that cast the 2-D sparse reconstruction problem as separate 1-D sparse reconstruction problems, thus effectively reducing the computational complexity. The offerings of the proposed technique were demonstrated by simulation results.

References

[1] S. Qin, Y. D. Zhang, and M. G. Amin, "Multi-target localization using frequency diverse coprime arrays with coprime frequency offsets," in *Proc. IEEE Radar Conf.*, Philadelphia, PA, 2016, pp. 1–5.

[2] M. Skolnik, *Radar Handbook, Third Edition*. McGraw-Hill, 2008.

[3] D. Ribas, P. Ridao, and J. Neira, *Underwater SLAM for Structured Environments Using an Imaging Sonar*. Springer, 2010.

[4] G. Mao and B. Fidan, Eds, *Localization Algorithms and Strategies for Wireless Sensor Networks*. Information Science Reference, 2009.

[5] C. Gentile, N. Alsindi, R. Raulefs, and C. Teolis, *Geolocation Techniques: Principles and Applications*. Springer, 2012.

[6] B. Bauman, A. Christianson, A. Wegener, and W. J. Chappell, "Dynamic visualization of antenna patterns and phased-array beam steering," *IEEE Antennas Propag. Mag.*, vol. 54, no. 3, pp. 184–193, 2012.

[7] P. Rocca, R. L. Haupt, and A. Massa, "Interference suppression in uniform linear arrays through a dynamic thinning strategy," *IEEE Trans. Antennas Propag.*, vol. 59, no. 12, pp. 4525–4533, 2011.

[8] J. R. Mosig, "An old tool and a new challenge for depicting antenna array radiation patterns," *IEEE Antennas Propag. Mag.*, vol. 53, no. 3, pp. 115–123, 2011.

[9] T. F. Chun, A. Zamora, J. L. Bao, R. T. Iwami, and W. A. Shiroma, "An interleaved, interelement phase-detecting/phase-shifting retrodirective antenna array for interference reduction," *IEEE Antennas Wirel. Propag. Lett.*, vol. 10, pp. 919–922, 2011.

[10] P. Antonik, M. C. Wicks, H. D. Griffiths, and C. J. Baker, "Frequency diverse array radars," in *Proc. IEEE Radar Conf.*, Verona, NY, 2006, pp. 215–217.

[11] M. Secmen, S. Demir, A. Hizal, and T. Eker, "Frequency diverse array antenna with periodic time modulated pattern in range and angle," in *Proc. IEEE Radar Conf.*, Boston, MA, 2007, pp. 427–430.

[12] P. Antonik, "An investigation of a frequency diverse array," Ph.D. dissertation, Univ. College London, London, U.K., 2009.

[13] W.-Q. Wang, "Phased-MIMO radar with frequency diversity for range-dependent beamforming," *IEEE Sens. J.*, vol. 13, no. 4, pp. 1320–1328, 2013.

[14] P. F. Sammartino, C. J. Baker, and H. D. Griffiths, "Frequency diverse MIMO techniques for radar," *IEEE Trans. Aerosp. Electron. Syst.*, vol. 49, no. 1, pp. 201–222, 2013.

[15] W.-Q. Wang and H. C. So, "Transmit subaperturing for range and angle estimation in frequency diverse array radar," *IEEE Trans. Signal Process.*, vol. 62, no. 8, pp. 2000–2011, 2014.

[16] W.-Q. Wang, "Frequency diverse array antenna: New opportunities," *IEEE Antennas Propag. Mag.*, vol. 57, no. 2, pp. 145–152, 2015.

[17] Z. Xiang and B. Chen, "Optimal frequency increment selection in frequency diverse multiple-input-multiple-output radar," *IET Radar Sonar Navig.*, DOI:10.1049/iet-rsn.2015.0519, 2016.

[18] K. Gao, W.-Q. Wang, and J. Cai, "Frequency diverse array and MIMO hybrid radar transmitter design via Cramer-Rao lower bound minimization," *IET Radar Sonar Navig.*, DOI:10.1049/iet-rsn.2015.0644, 2016.

[19] W. Khan, I. M. Qureshi, A. Basit, and W. Khan, "Range-bins-based MIMO frequency diverse array radar with logarithmic frequency offset," *IEEE Antennas Wirel. Propag. Lett.*, vol. 15, pp. 885–888, 2016.

[20] W.-Q. Wang, "Moving-target tracking by cognitive RF stealth radar using frequency diverse array antenna," *IEEE Trans. Geosci. Remote Sens.*, vol. 54, no. 7, pp. 3764–3773, 2016.

[21] J. Xu, G. Liao, S. Zhu, L. Huang, and H. C. So, "Joint range and angle estimation using MIMO radar with frequency diverse array," *IEEE Trans. Signal Process.*, vol. 63, no. 13, pp. 3396–3410, 2015.

[22] K. Gao, H. Shao, H. Chen, J. Cai and W. -Q. Wang, "Impact of frequency increment errors on frequency diverse array MIMO in adaptive beamforming and target localization," *Digital Signal Process.*, vol. 44, pp. 58–67, 2015.

[23] W.-Q. Wang and H. Shao, "Range-angle localization of targets by a double-pulse frequency diverse array radar," *IEEE J. Sel. Top. Signal Process.*, vol. 8, no. 1, pp. 106–114, 2014.

[24] R. T. Hoctor and S. A. Kassam, "The unifying role of the coarray in aperture synthesis for coherent and incoherent imaging," *Proc. IEEE*, vol. 78, no. 4, pp. 735–752, 1990.

[25] W.-Q. Wang, H. C. So, and H. Shao, "Nonuniform frequency diverse array for range-angle imaging of targets," *IEEE Sens. J.*, vol. 14, no. 8, pp. 2469–2476, 2014.

[26] P. Pal and P. P. Vaidyanathan, "Nested arrays: A novel approach to array processing with enhanced degrees of freedom," *IEEE Trans. Signal Process.*, vol. 58, no. 8, pp. 4167–4181, 2010.

[27] P. P. Vaidyanathan and P. Pal, "Sparse sensing with co-prime samplers and arrays," *IEEE Trans. Signal Process.*, vol. 59, no. 2, pp. 573–586, 2011.

[28] Y. D. Zhang, M. G. Amin, F. Ahmad, and B. Himed, "DOA estimation using a sparse uniform linear array with two CW signals of co-prime frequencies," in *Proc. IEEE Workshop Comput. Adv. Multi-sensor Adapt. Process. (CAMSAP)*, Saint Martin, 2013, pp. 404–407.

[29] Q. Wu and Q. Liang, "Coprime sampling for nonstationary signal in radar signal processing," *EURASIP J. Wireless Commun. Netw.*, vol. 2013, no. 58, pp. 1–11, 2013.

[30] J. Chen, Q. Liang, B. Zhang and X. Wu, "Spectrum efficiency of nested sparse sampling and coprime sampling," *EURASIP J. Wireless Commun. Netw.*, vol. 2013, no. 47, pp. 1–15, 2015.

[31] K. Adhikari, J. R. Buck and K. E. Wage, "Extending coprime sensor arrays to achieve the peak side lobe height of a full uniform linear array," *EURASIP J. Adv. Signal Process.*, vol. 2014, no. 148, pp. 1-17, 2014.

[32] Z. Tan and A. Nehorai, "Sparse direction-of-arrival estimation using co-prime arrays with off-grid targets," *IEEE Signal Process. Lett.*, vol. 21, no. 1, pp. 26–29, 2014.

[33] Z. Tan, Y. Eldar, and A. Nehorai, "Direction of arrival estimation using co-prime arrays: A super resolution viewpoint," *IEEE Trans. Signal Process.*, vol. 62, no. 21, pp. 5565–5576, 2014.

[34] S. Qin, Y. D. Zhang, and M. G. Amin, "Generalized coprime array configurations for direction-of-arrival estimation," *IEEE Trans. Signal Process.*, vol. 63, no. 6, pp. 1377–1390, 2015.

[35] S. Qin, Y. D. Zhang, Q. Wu, and M. G. Amin, "Structure-aware Bayesian compressive sensing for near-field source localization based on sensor-angle distributions," *Int. J. Antennas Propag.*, vol. 2015, article ID 783467, 2015.

[36] C. L. Liu and P. P. Vaidyanathan, "Coprime arrays and samplers for space-time adaptive processing," in *Proc. IEEE Int. Conf. Acoust. Speech Signal Process. (ICASSP)*, Brisbane, Australia, 2015, pp. 2364–2368.

[37] S. Qin, Y. D. Zhang, and M. G. Amin, "Sparsity-based multi-target localization exploiting multi-frequency coprime array," in *Porc. IEEE China Summit and Int. Conf. Signal and Inform. Process. (ChinaSIP)*, Chengdu, China, 2015, pp. 329–333.

[38] Q. Shen, W. Liu, W. Cui, S. Wu, Y. D. Zhang, and M. G. Amin, "Low-complexity wideband direction-of-arrival estimation based on co-prime arrays," *IEEE/ACM Trans. Audio, Speech and Language Process.*, vol. 23, no. 9, pp. 1445–1456, 2015.

[39] S. Qin, Y. D. Zhang, M. G. Amin, and A. Zoubir, "Generalized coprime sampling of Toeplitz matrices," in *Proc. IEEE Int. Conf. Acoust. Speech Signal Process. (ICASSP)*, Shanghai, China, 2016, pp. 4468–4472.

[40] S. Qin, Y. D. Zhang, M. G. Amin, and B. Himed, "DOA estimation exploiting a uniform linear array with multiple co-prime frequencies," *Signal Process.*, vol. 130, pp. 37-46, 2017.

[41] S. Qin, Y. D. Zhang, M. G. Amin, and A. Zoubir, "Generalized coprime sampling of Toeplitz matrix," *IEEE Trans. Signal Process.*, in press.

[42] W.-Q. Wang and C. Zhu, "Nested array receiver with time-delayers for joint target range and angle estimation," *IET Radar Sonar Navig.*, DOI:10.1049/iet-rsn.2015.0450, 2016.

[43] J. Xiong, W.-Q. Wang, H. Chen, and H. Shao, "Compressive sensing-based range and angle estimation for nested FDA radar," in *Proc. Asia-Pacific Signal Inf. Process. Assoc. Annu. Summit Conf. (APSIPA)*, 2015, pp. 608-611.

[44] D. L. Donoho, "Compressed sensing," *IEEE Trans. Inf. Theory*, vol. 52, no. 4, pp. 1289–1306, 2006.

[45] D. Wipf and S. Nagarajan, "Beamforming using the relevance vector machine," in *Proc. Int. Conf. Mach. Learn.*, Corvallis, OR, 2007, pp. 1023–1030.

[46] S. Ji, Y. Xue, and L. Carin, "Bayesian compressive sensing," *IEEE Trans. Signal Process.*, vol. 56, no. 6, pp. 2346–2356, 2008.

[47] S. Ji, D. Dunson, and L. Carin, "Multitask compressive sensing," *IEEE Trans. Signal Process.*, vol. 57, no. 1, pp. 92–106, 2009.

[48] Z. Yang, L. Xie, and C. Zhang, "Off-grid direction-of-arrival estimation using sparse Bayesian inference," *IEEE Trans. Signal Process.*, vol. 61, no. 1, pp. 38–43, 2013.

[49] Q. Wu, Y. D. Zhang, and M. G. Amin, "Complex multitask Bayesian compressive sensing," in *Proc. IEEE Int. Conf. Acoust. Speech Signal Process. (ICASSP)*, Florence, Italy, 2014, pp. 3375–3379.

[50] X. Wang, M. G. Amin, F. Ahmad, and E. Aboutanios, "Bayesian compressive sensing for DOA estimation using the difference coarray," in *Proc. IEEE Int. Conf. Acoust. Speech Signal Process. (ICASSP)*, Brisbane, Australia, 2015, pp. 2384–2388.

[51] Q. Wu, Y. D. Zhang, M. G. Amin, and B. Himed, "Multi-task Bayesian compressive sensing exploiting intra-task dependency," *IEEE Signal Process. Lett.*, vol. 22, no. 4, pp. 430–434, 2015.

[52] R. Klemm, *Space-Time Adaptive Processing: Principles and Applications*. IEEE Press, 1998.

[53] J. W. Odendaal, E. Barnard, and C. W. I. Pistorius, "Two-dimensional superresolution radar imaging using the MUSIC algorithm," *IEEE Trans. Antennas Propag.*, vol. 42, no. 10, pp. 1386–1391, 1994.

[54] X-G. Xia and G. Wang, "Phase unwrapping and a robust Chinese remainder theorem," *IEEE Signal Process. Lett.*, vol. 14, no. 4, pp. 247–250, 2007.

[55] P. Pal and P. P. Vaidyanathan, "Coprime sampling and the MUSIC algorithm," in *Proc. IEEE Digital Signal Process. Workshop and IEEE Signal Process. Educ. Workshop (DSP/SPE)*, Sedona, AZ, 2011, pp. 289–294.

[56] Y. D. Zhang, S. Qin, and M. G. Amin, "DOA estimation exploiting coprime arrays with sparse sensor spacing," in *Proc. IEEE Int. Conf. Acoust. Speech Signal Process. (ICASSP)*, Florence, Italy, 2014, pp. 2267–2271.

[57] T.-J. Shan, M. Wax, and T. Kailath, "On spatial smoothing for direction-of-arrival estimation of coherent signals," *IEEE Trans. Acoust. Speech Signal Process.*, vol. 33, no. 4, pp. 806–811, 1985.

[58] Y. M. Chen, "On spatial smoothing for two-dimensional direction-of-arrival estimation of coherent signals," *IEEE Trans. Signal Process.*, vol. 45, no. 7, pp. 1689–1696, 1997.

[59] Y. D. Zhang, M. G. Amin, and B. Himed, "Sparsity-based DOA estimation using co-prime arrays," in *Proc. IEEE Int. Conf. Acoust. Speech Signal Process. (ICASSP)*, Vancouver, Canada, 2013, pp. 3967–3971.

[60] R. Jagannath and K. Hari, "Block sparse estimator for grid matching in single snapshot DOA estimation," *IEEE Signal Process. Lett.*, vol. 20, no. 11, pp. 1038–1041, 2013.

[61] Z. Tan, P. Yang, and A. Nehorai, "Joint sparse recovery method for compressed sensing with structured dictionary mismatch," *IEEE Trans. Signal Process.*, vol. 62, no. 19, pp. 4997–5008, 2014.

[62] M. E. Tipping, "Sparse Bayesian learning and the relevance vector machine," *J. Mach. Learn. Res.*, vol. 1, no. 9, pp. 211–244, 2001.

[63] S. D. Babacan, R. Molina, and A. K. Katsaggelos, "Bayesian compressive sensing using Laplace priors," *IEEE Trans. Image Process.*, vol. 19, no. 1, pp. 53–63, 2010.

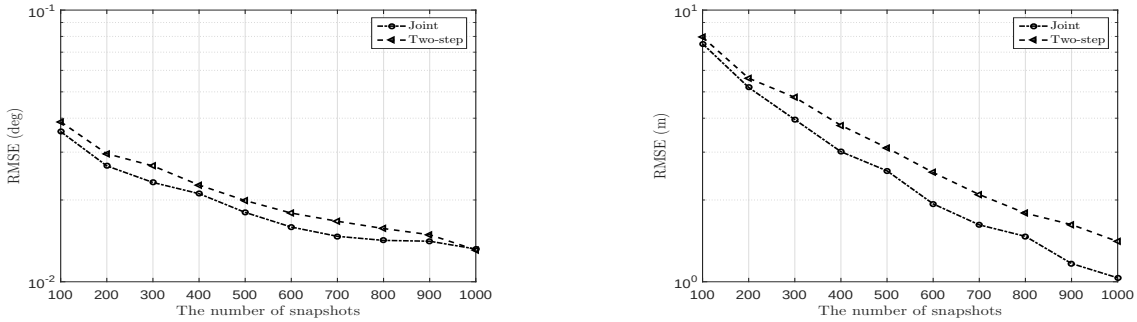

Fig. 6. RMSE versus the number of snapshots using the joint and two-step estimation methods ($Q = 2$ and SNR$= -5$ dB). (a) RMSE_θ; (b) RMSE_R

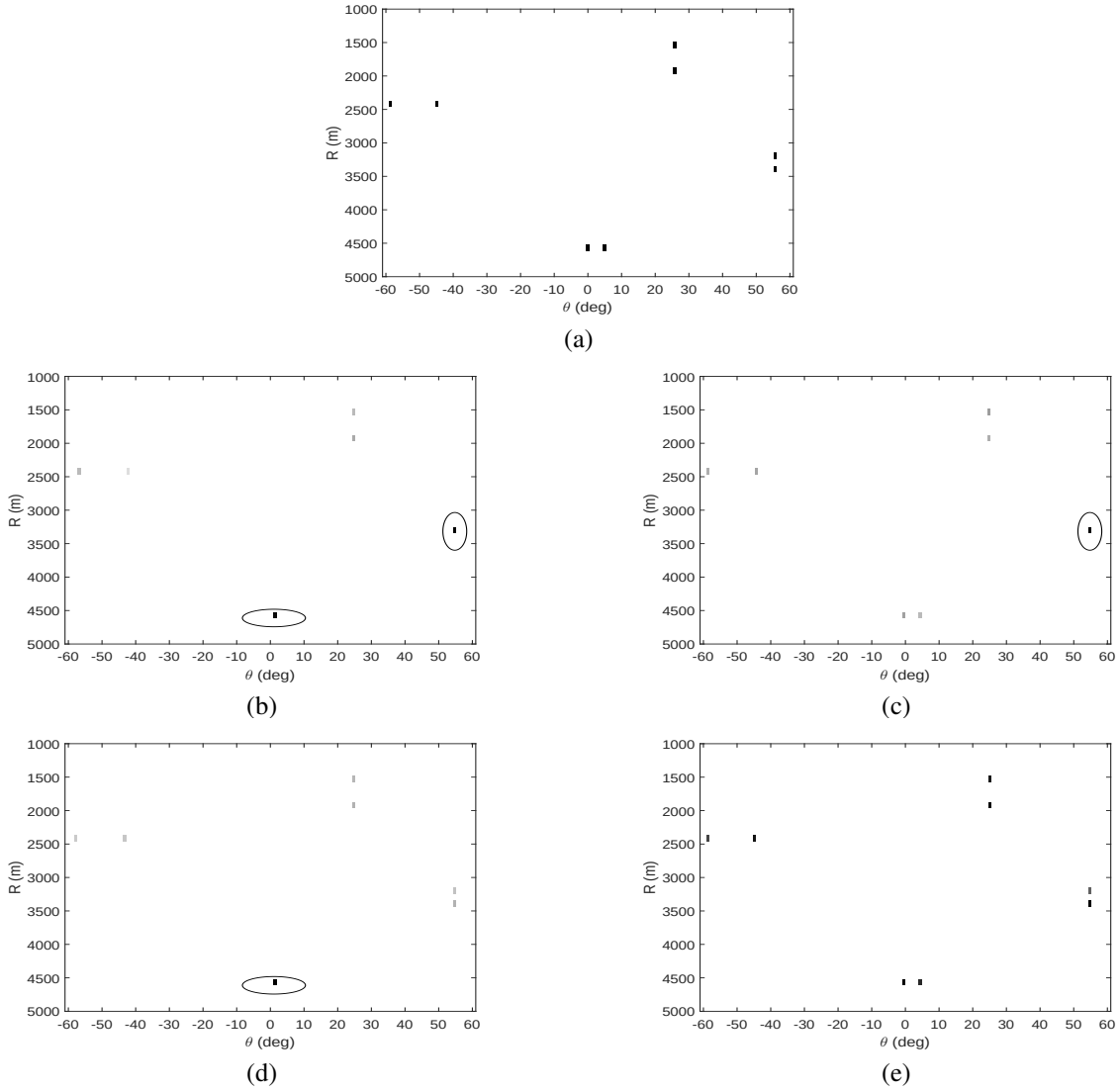

Fig. 7. The localization results using different schemes ($Q = 8$) (a) True; (b) ULA-UFO; (c) CA-UFO; (d) ULA-CFO; (e) CA-CFO.

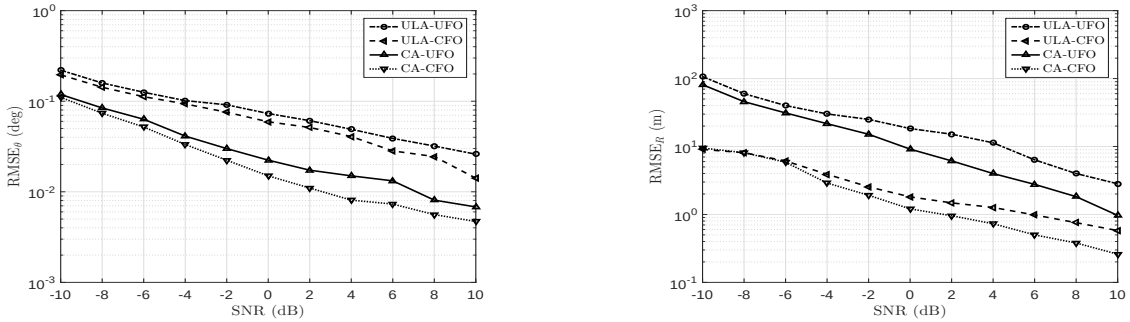

Fig. 8. RMSE versus SNR ($Q = 2$ and $T = 500$). (a) RMSE_θ; (b) RMSE_R

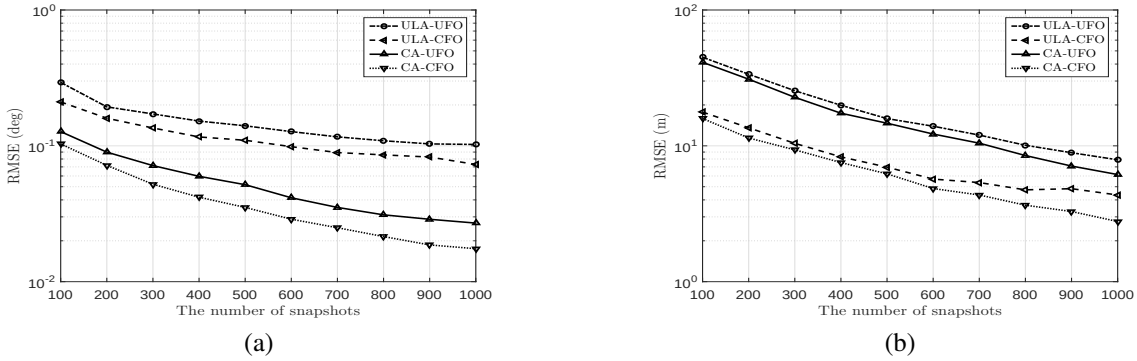

Fig. 9. RMSE versus the number of snapshots ($Q = 2$ and SNR$= -5$ dB). (a) RMSE_θ; (b) RMSE_R

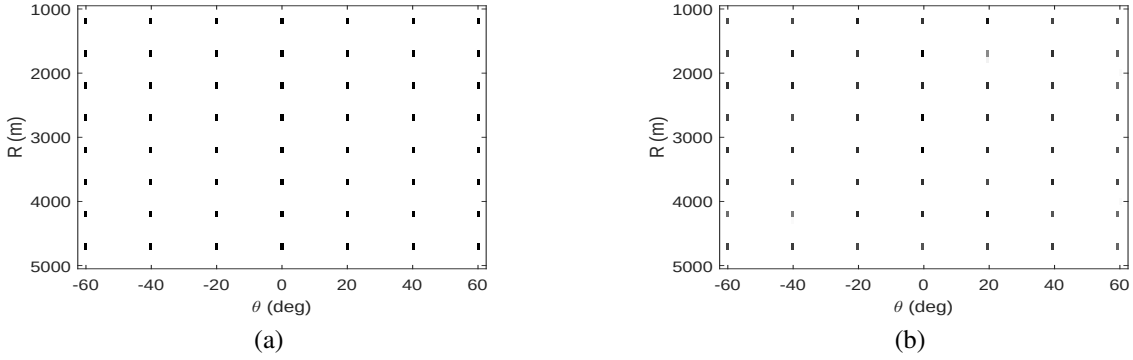

Fig. 10. The localization results using CA-CFO ($Q = 56$). (a) True; (b) Estimated

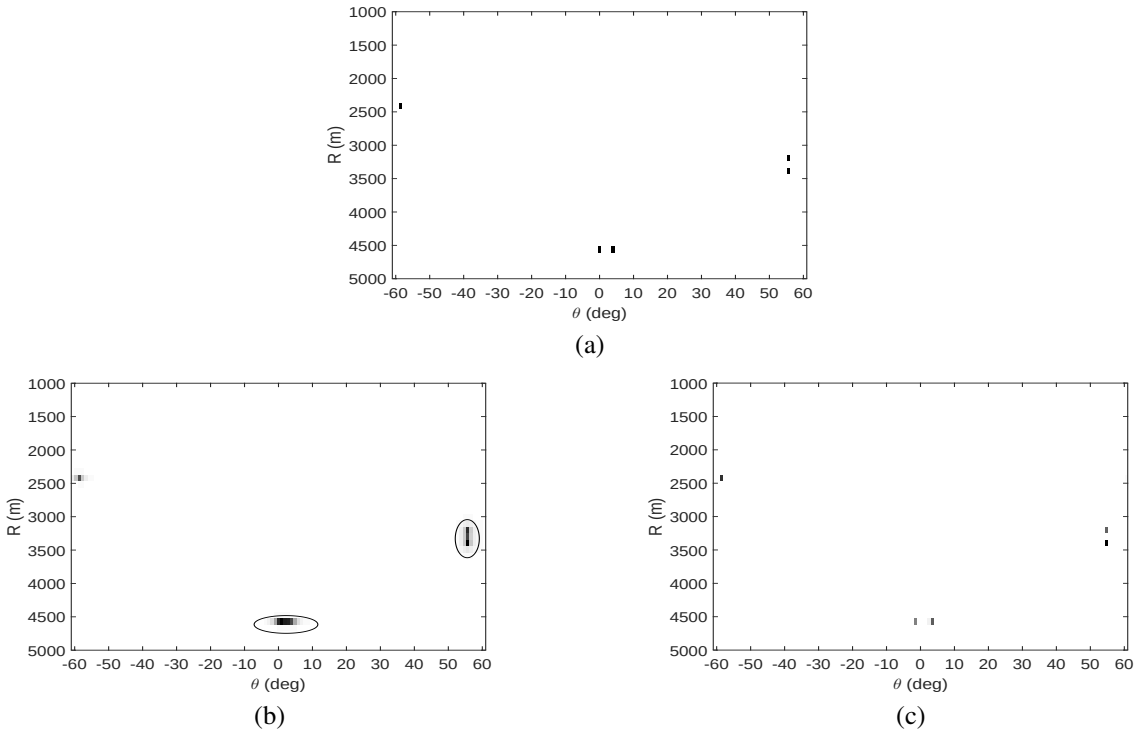

Fig. 11. The localization results for different methods using CA-CFO ($Q = 5$, $T = 500$, and SNR= 0 dB) (a) True; (b) MUSIC-SS; (c) Proposed.

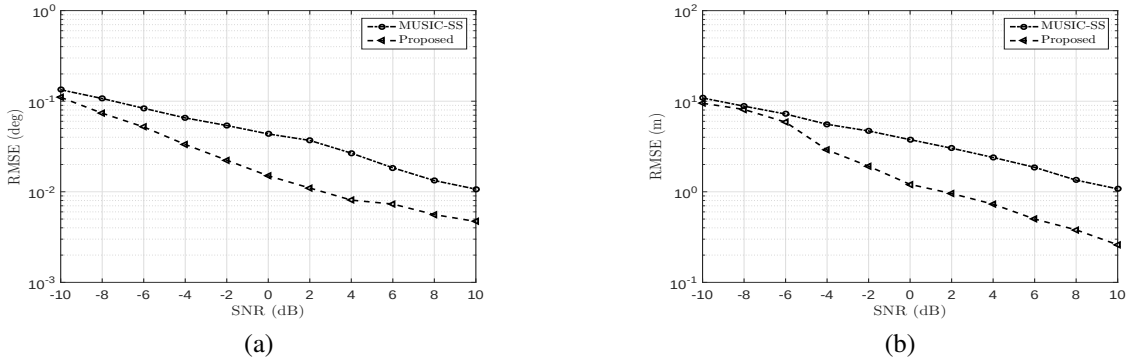

Fig. 12. RMSE versus SNR for different methods using CA-CFO ($Q = 2$ and $T = 500$). (a) RMSE_θ; (b) RMSE_R

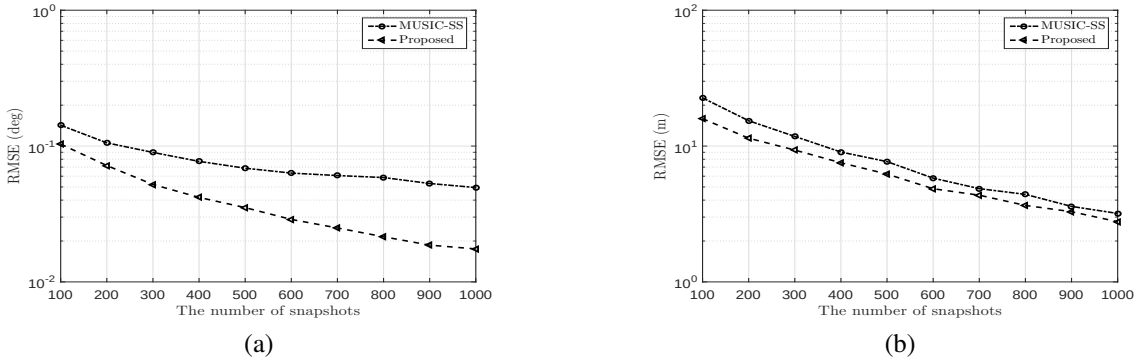

Fig. 13. RMSE versus the number of snapshots for different methods using CA-CFO ($Q = 2$ and SNR$= -5$ dB). (a) RMSE_θ; (b) RMSE_R

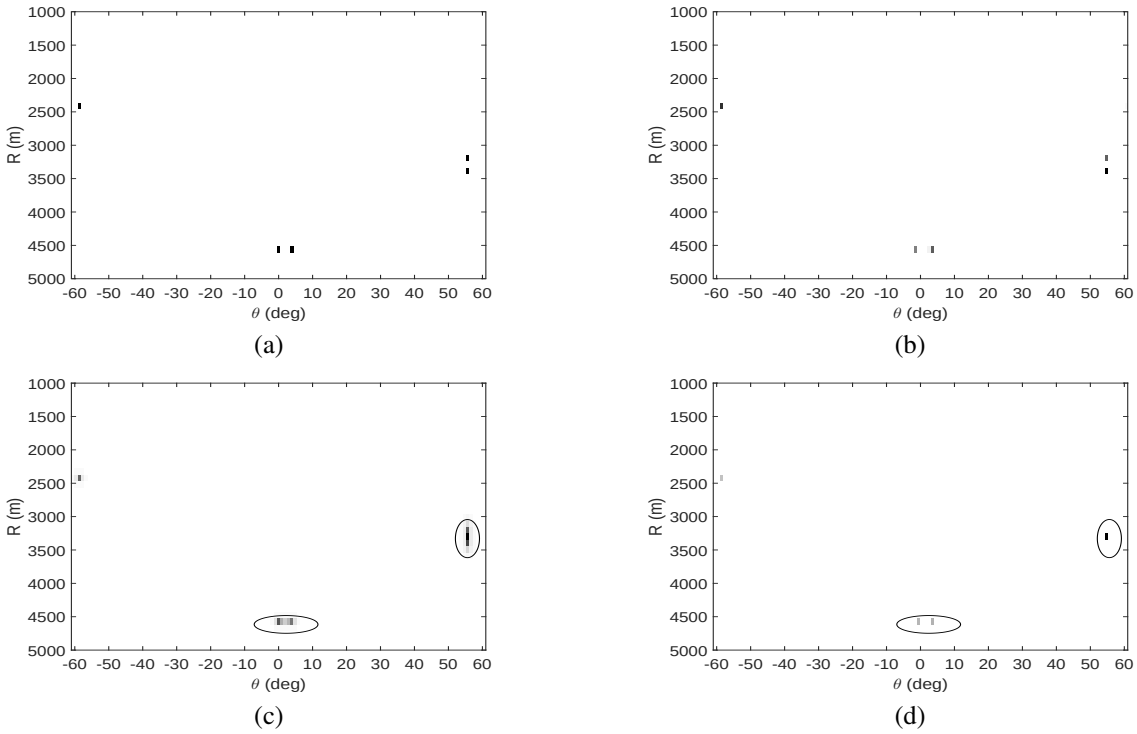

Fig. 14. The localization results for different methods ($Q = 5$, $T = 500$, and SNR= 0 dB) (a) True; (b) Proposed; (c) Nested-MUSIC; (d) Nested-CS.

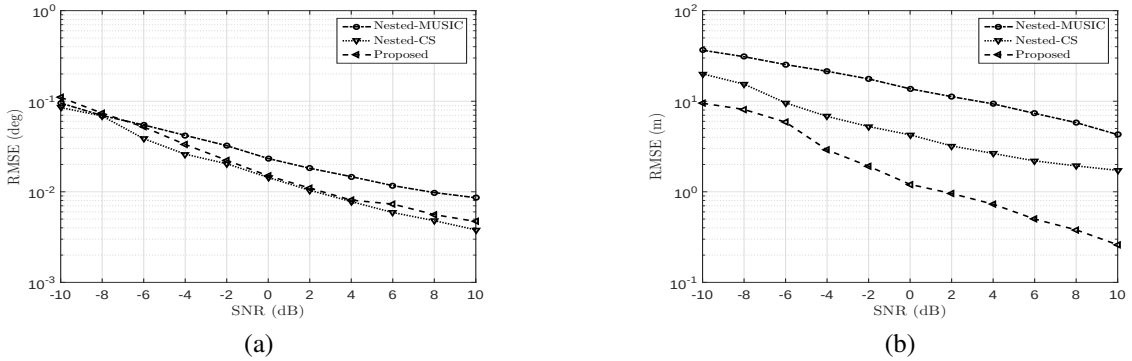

Fig. 15. RMSE versus the SNR for different methods ($Q = 2$ and $T = 500$). (a) RMSE_θ; (b) RMSE_R

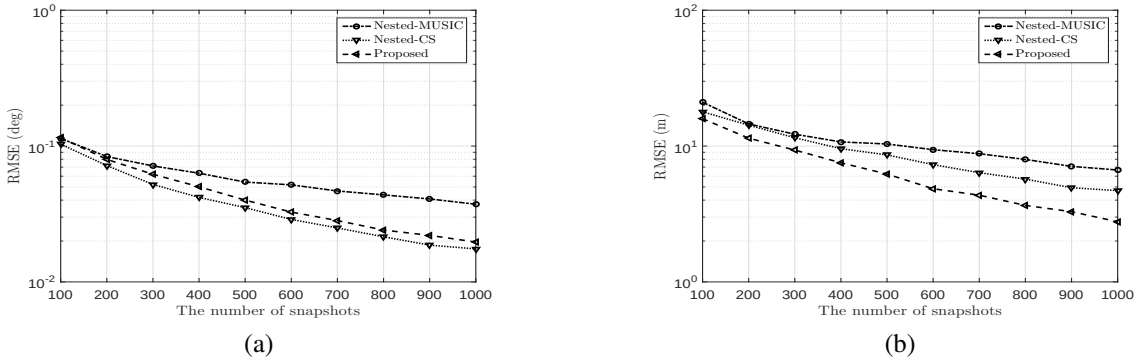

Fig. 16. RMSE versus the number of snapshots for different methods ($Q = 2$ and SNR$= -5$ dB). (a) RMSE_θ; (b) RMSE_R

Si Qin received the B.S. and M.S. degrees in Electrical Engineering from Nanjing University of Science and Technology, Nanjing, China, in 2010 and 2013, respectively. Currently, he is a Research Assistant at the Center for Advanced Communications, Villanova University, Villanova, PA, working toward his Ph.D. degree in Electrical Engineering. His research interests include direction-of-arrival estimation, sparse array and signal processing, and radar signal processing.

Mr. Si Qin received the First Prize of Student Paper Competition at 2014 IEEE Benjamin Franklin Symposium on Microwave and Antenna Sub-systems (BenMAS) and Best Student Paper Award at 2012 IEEE International Conference on Microwave and Millimeter Wave Technology (ICMMT).

Yimin D. Zhang (SM'01) received his Ph.D. degree from the University of Tsukuba, Tsukuba, Japan, in 1988.

Dr. Zhang joined the faculty of the Department of Radio Engineering, Southeast University, Nanjing, China, in 1988. He served as a Director and Technical Manager at the Oriental Science Laboratory, Yokohama, Japan, from 1989 to 1995, a Senior Technical Manager at the Communication Laboratory Japan, Kawasaki, Japan, from 1995 to 1997, and a Visiting Researcher at the ATR Adaptive Communications Research Laboratories, Kyoto, Japan, from 1997 to 1998. He was with the Villanova University, Villanova, PA, USA, from 1998 to 2015, where he was a Research Professor with the Center for Advanced Communications. Since 2015, he has been with the Department of Electrical and Computer Engineering, College of Engineering, Temple University, Philadelphia, PA, USA, where he is currently an Associate Professor. His general research interests lie in the areas of statistical signal and array processing applied to radar, communications, and navigation, including compressive sensing, convex optimization, time-frequency analysis, MIMO system, radar imaging, target localization and tracking, wireless networks, and jammer suppression. He has published more than 300 journal articles and conference papers and 12 book chapters. Dr. Zhang received the 2016 Premium Award from the Institution of Engineering and Technology (IET) for Best Paper published in *IET Radar, Sonar & Navigation*.

Dr. Zhang is a member of the Sensor Array and Multichannel (SAM) Technical Committee of the IEEE Signal Processing Society. He is an Associate Editor for the IEEE TRANSACTIONS ON SIGNAL PROCESSING, and serves on the Editorial Board of the *Signal Processing* journal. He was an Associate Editor for the IEEE SIGNAL PROCESSING LETTERS during 2006–2010, and an Associate Editor for the *Journal of the Franklin Institute* during 2007–2013.

Moeness G. Amin (F'01) received the Ph.D. degree in electrical engineering from the University of Colorado, Boulder, CO, USA, in 1984. Since 1985, he has been with the Faculty of the Department of Electrical and Computer Engineering, Villanova University, Villanova, PA, USA, where he became the Director of the Center for Advanced Communications, College of Engineering, in 2002. Dr. Amin is a Fellow of the Institute of Electrical and Electronics Engineers; Fellow of the International Society of Optical Engineering; Fellow of the Institute of Engineering and Technology (IET), and a Fellow of the European Association for Signal Processing (EURASIP). Dr. Amin is the Recipient of the 2016 Alexander von Humboldt Research Award, the 2016 IET Achievement Medal, the 2014 IEEE Signal Processing Society Technical Achievement Award, the 2009 Individual Technical Achievement Award from the European Association for Signal Processing, the 2015 IEEE Aerospace and Electronic Systems Society Warren D. White Award for Excellence in Radar Engineering, the IEEE Third Millennium Medal, the 2010 NATO Scientific Achievement Award, and the 2010 Chief of Naval Research Challenge Award. He is the recipient of the 1997 Villanova University Outstanding Faculty Research Award and the 1997 IEEE Philadelphia Section Award. He was a Distinguished Lecturer of the IEEE Signal Processing Society, 2003-2004, and is presently the Chair of the Electrical Cluster of the Franklin Institute Committee on Science and the Arts. Dr. Amin has over 700 journal and conference publications in signal processing theory and applications. He co-authored 20 book chapters and is the Editor of the three books *Through the Wall Radar Imaging*, *Compressive Sensing for Urban Radar*, and *Radar for Indoor Monitoring* published by CRC Press in 2011, 2014, and 2017, respectively.

Fulvio Gini (F) received the Doctor Engineer (cum laude) and the Research Doctor degrees in electronic engineering from the University of Pisa, Italy, in 1990 and 1995, respectively. In 1993 he joined the Department of Ingegneria dellInformazione of the University of Pisa, where he become Associate Professor in 2000 and he is Full Professor since 2006. From July 1996 through January 1997, he was a visiting researcher at the Department of Electrical Engineering, University of Virginia, Charlottesville. He is an Associate Editor for the IEEE Transactions on Aerospace and Electronic Systems since January 2007 and for the Elsevier Signal Processing journal since December 2006. He has been AE for the IEEE Transactions on Signal Processing (2000-2006) and a Senior AE of the same Transactions since February 2016. He was a Member of the EURASIP JASP Editorial Board. He was co-founder and 1st co-Editor-in-Chief of the Hindawi International Journal on Navigation and Observation (2007–2011). He is the Area Editor for the Special issues of the IEEE Signal Processing Magazine. He was co-recipient of the 2001 IEEE AES Societys Barry Carlton Award for Best Paper. He was recipient of the 2003 IEE Achievement Award for outstanding contribution in signal processing and of the 2003 IEEE AES Society Nathanson Award to the Young Engineer of the Year. He is Member of the Radar System Panel of the IEEE Aerospace and Electronic Systems Society (AESS) (2008–present). He is a member of the IEEE SPS Awards Board. He has been a Member of the Signal Processing Theory and Methods (SPTM) Technical Committee (TC) of the IEEE Signal Processing Society and of the Sensor Array and Multichannel (SAM) TC for many years. He is a Member of the Board of Directors (BoD) of the EURASIP Society, the Award Chair (2006-2012) and the EURASIP President for the years 2013-2016. He was the Technical co-Chair of the 2006 EURASIP Signal and Image Processing Conference (EUSIPCO 2006), Florence (Italy), of the 2008 Radar Conference, Rome (Italy), and of the 2015 IEEE CAMSAP workshop, Cancun (Mexico). He was the General co-Chair of the 2nd Workshop on Cognitive Information Processing (CIP2010), of the IEEE ICASSP 2014, held in Florence (Italy), and of the 2nd, 3rd and 4th editions of the workshop on Compressive Sensing in Radar (CoSeRa). He was the guest co-editor of the special section of the Journal of the IEEE SP Society on Special Topics in Signal Processing on "Adaptive Waveform Design for Agile Sensing and Communication" (2007), guest editor of the special section of the IEEE Signal Processing Magazine on "Knowledge Based Systems for Adaptive Radar Detection, Tracking and Classification" (2006), guest co-editor of the two special issues of the EURASIP Signal Processing journal on "New trends and findings in antenna array processing for radar" (2004) and on "Advances in Sensor Array Processing (in memory of Alex Gershman)" (2013). He is co-editor and author of the book *Knowledge Based Radar Detection, Tracking and Classification* (2008) and of the book *Waveform Diversity and Design* (2012). He authored or co-authored 9 book chapters, more than 120 journal papers and more than 155 conference papers.